Modelling and Mathematical Analysis of Quantum Systems at the Nanoscale

Asma Jazza Alanazy

PhD Thesis in Mathematics

Lancaster University

Submitted in partial fulfilment of the requirements for the degree of Doctor of Philosophy

Septemper 2019

Declaration

Except where stated otherwise, this thesis is a result of the author's original work and has not been submitted in whole or in part for the award of a higher degree elsewhere. This thesis documents work carried out between October 2016 and March 2019 at Lancaster University, UK, under the supervision of Prof. Colin J. Lambert and funded by Northern-border University, Saudi Arabia.

Asma Alanazy

September 2019

I dedicate this thesis to

My beloved parents and husband, My Kids

For their love, endless support, Encouragement and sacrifices.

Abstract

When a single molecule is connected to external electrodes by linker groups, the connectivity of the linkers to the molecular core can be controlled to atomic precision by appropriate chemical synthesis. Recently, the connectivity dependence of the electrical conductance of single molecules has been investigated both theoretically and experimentally. Green's function plays a significant role in determining the transmissions coefficients. The study presents the Landauer formula and Green's function approach for analysing the scattering processes in a system attached to infinite one-dimensional leads. The study involves the calculation of the retarded Green's function in which the simple formula of a one-dimensional tight binding chain in presented. The periodicity of the lattice is also broken at a single connection for showing the Green's function associated with the transmission coefficient along the scattering region.

In chapter 3 I study the connectivity dependence of the Wigner delay time of single-molecule. This chapter addresses the question of the time spent by a transmitted wave packet within a scattering region. The study involves mathematical aspects of solving the Schrodinger equation in open systems with a view to developing new conceptual approaches to scattering theory. Efficient schemes to obtain scattering matrices from mean-field Hamiltonians are developed and these are implemented in new numerical codes. The relationship between the phase of S-matrix elements and Wigner delay times is also elucidated.

To analyse delay times in bipartite lattices, tight binding calculations are used and a new computer code is developed to verify analytical predictions. In particular, Green's functions and a mid-gap theory are used to calculate Wigner delay times for different connectivities in graphene like molecules. One interesting and counterintuitive result is that in the weak coupling limit at the middle of HOMO and LUMO gap, the Wigner delay time does not depend on the distance between the connections to external reservoirs.

A key goal in molecular electronics has been to find molecules that facilitate efficient charge transport over long distances. Normally molecular wires become less conductive with increasing length. Here in chapter 4 I report a series of fused porphyrin oligomers for which the conductance increases substantially with length by > 10-fold at a bias of 0.7 V. This exceptional behaviour can be attributed to the rapid decrease of the HOMO-LUMO gap with the length of fused porphyrins. In contrast, for butadiyne-linked porphyrin oligomers with moderate inter-ring coupling, a normal conductance decrease with length is found for all bias voltages explored (± 1 V). Further theoretical analysis using density functional theory underlines the role of inter-site coupling and indicates that this large increase in conductance with length at increasing voltages can be generalized to other molecular oligomers.

Charge transport through *meta*-connected biphenylene is strongly suppressed by destructive quantum interference (DQI) and as I demonstrate in chapter 5, this suppression persists when a saturated tetrahedral carbon is added to bridge the biphenyl moiety yielding a fluorene. In contrast, I demonstrate that DQI can be almost completely removed, and the electrical conductance boosted by almost a factor of 30, by adding a bridging carbonyl to yield a cross-conjugated fluorenone. This behavior is in marked contrast with other pi systems, such as para-connected anthraquinone, where cross-conjugation decreases the conductance. As a result of this conductance boost, when the

bridge is a carbonyl group, the conductance ratio of *meta* and *para* connected molecules is only a factor of 3. In contrast, in the fluorenes, when the bridge is a saturated tetrahedral carbon a large (ca. 100-fold) decrease in conductance is observed for *meta* compared with *para* connectivity. These conclusions on a family of eight fluorene and fluorenone derivatives with thioacetate and pyridine anchor groups with transport calculations are based on density functional theory and a simple tight-binding model, which reveal that any bridge atom alleviates the DQI to some degree and that the effect is greatest when the bridge atom is strongly coupled to the biphenylene unit. This result demonstrates that the carbonyl groups in *meta*-connected fluorenone wires increase the end-to-end coupling, even though the pendant groups are formally cross-conjugated.

Acknowledgements

" Above all, my great thanks to ALLAH for his mercy and blessing "

I would like to express deepest gratitude to my advisor Prof. Colin John Lambert for his full support and excellent supervision and expert guidance. This thesis would never have been completed without the advices I received from him. Colin, I know all words that I own would not express my gratitude to you, really it is honour for me to be under your supervision and to be a member of your research group.

I would like to take this opportunity to thank my co- supervisor Dr Sara Sangtarash for the great explanation and helpful guidance I received from her and for being ever so kind to show interest in my research. Sara, you assisted me with a great advices and reasonable feedback to improve my work within these years that I spent to complete this thesis.

I am also so grateful for Dr Hatef Sedeghi for providing the helpful tutorials and kind advices, and his interest for me and for everyone in the group.

I would like to thank my collaborating experimental group in (Liverpool and Oxford Universities).

I would like to thank my sponsor; Saudi Arabian Ministry of Higher Education & Scientific research for the sponsor me to study a PhD in the United Kingdom.

I also would like to extend my gratitude to **all** my PhD colleagues in Colin's group and to my lovely friend "Norah Algethami" for her kind help and support.

Unlimited thanks to my family. My Parents, you have done a lot to me, I hope you are proud of me and I wish one day I will be able to give you back. My beloved husband "Nasser" who gives me the largest support, endless love, care and encouragement to complete my study and carry on to achieve my dream. My lovely children, Majed and Mohammed certainly you are my whole life and the secret of my happiness. Also, I would like to express my very deep respect and sincere appreciation to my sisters and brothers, for their moral encouragement I received from them and for giving me so much love and support.

Publications

1. Edmund Leary., Bart Limburg., **Asma Alanazy.,** Sara Sangtarash., Iain Grace., Katsutoshi Swada., Louisa J. Esdaile., Mohammed Noori., M. Teresa González., Gabino Rubio-Bollinger., Hatef Sadeghi., Andrew Hodgson., Nicolás Agrait., Simon J. Higgins., Colin J. Lambert., Harry L. Anderson., and Richard J. Nichols. (2018). Bias-driven conductance *increase* with length in porphyrin tapes. *J. Am. Chem. Soc. 2018, 140, 12877−12883*

2. **Asma Alanazy.,** Edmund Leary., Takayuki Kobatake., Sara Sangtarash., M. Teresa González., Hua-Wei Jiang., Gabino Rubio-Bollinger., Nicolás Agrait ., Hatef Sadegh., Iain Grace., Simon J. Higgins ., Harry L. Anderson ., Richard J. Nichols., and Colin J. Lambert. (2019). Cross conjugation increases the conductance of *meta*-connected fluorenones. (submitted).

3. P. Rakyta., **A. Alanazy.,** A. Kormányos., Z. Tajkov., G. Kukucska., J. Koltai., S. Sangtarash., H. Sadeghi., J. Cserti and C.J. Lambert. (2019). Magic number theory of superconducting proximity effects and Wigner delay times in graphene-like molecules. (submitted).

Table of Contents

1. Introduction 11

1.1. Molecular scale electronics 11

1.2. Thesis outline 15

Bibliography 17

2. Chapter 2: Theory of single particle transport 21

2.1. Introduction 21

2.2. The Landauer formula 22

2.3. Theory of electron transport 25

2.4. Scattering theory 26

2.4.1. One dimensional (1-D) linear crystalline lattice 26

2.4.2. Semi-infinite one-dimensional lattice 30

2.4.3. One-dimensional (1-D) scattering 32

2.4.4. One-dimensional (1-D) Scattering Using Green's functions 32

2.5. More general method to calculate the transmission from wave function 35

2.5.1. Schrödinger equation representation 35

2.6. Features of the transmission curve 39

2.6.1. Breit-Wigner Resonance 39

2.6.2. Fano Resonances 43

2.6.3. Anti-Resonances 44

Bibliography 46

3. Chapter 3: Wigner delay time in graphene-like Molecules 48

3.1. Introduction 49

3.2. Method 49
3.3. Results and discussion 55
3.4. Calculation of the Wigner delay times for on-resonance transport 59
Bibliography 65

4. Chapter 4: Bias-driven conductance *increase* with length in porphyrin tapes 69
4.1. Introduction 70
4.2. Molecular structure 72
4.3. Results and discussion 74
Bibliography 76

5. Chapter 5: Cross conjugation increases the conductance of *meta*-connected fluorenones 81
5.1. Introduction 82
5.2. Molecular structure 83
5.3. Results and discussion 86
Bibliography 93

6. Chapter 6: Conclusion and future work 99
5.1. Conclusion 99
5.2. Future work 101
Bibliography 102

Chapter 1

Introduction

1.1 Molecular scale electronics

In recent years much emphasis has been given to understanding the electronic structure and uncovering the properties of single molecules[1]. The field of molecular electronics is based on exploiting molecules as fundamental units for computing and other electronic functions. Which gives molecular electronics an attractive role in the field of technology because it provides the ultimate size for system scaling[2]. The dimensions of some molecular systems are a few nanometres, and therefore molecular electronics should be viewed as a subfield of nanotechnology[3]. The idea of using single molecules as building blocks to design and fabricate molecular electronic components has been around for more than 40 years[4], but only recently has attracted huge scientific interest to explore their unique properties and opportunities. Improvement in the methods used to calculate molecular electronic properties allows theorists to deal with more complicated molecules and to match their calculations more closely to reality as experimental groups across the world use a variety of measurement techniques to study the molecule's electronic properties. The motivation behind the collaboration between theory and experiment is twofold, due to the simple fact that the minute size of the molecules makes it unclear to experimentalists what exactly is being measured, e.g. how the molecule is orientated or

connected to the electrodes, this can be resolved by modelling the structure using density functional theory, (DFT) which is implemented in the SIESTA code[5], and the non-equilibrium Green's function formalism of transport theory[6], which is implemented in the Gollum code[7] together providing an explanation of the experimental data from the theoretical calculations.

Molecular electronics is a modern technique and a single electron transistor is still to appear on an industrial scale, but a number of other interesting effects have been observed in experiment and theory including self-assembled monolayers.[8] Single-molecule junctions[9] are of interest not only for their potential to deliver logic gates[10] , sensors[11] and memories,[12] but also for their ability to probe room-temperature quantum properties at a molecular scale such as quantum interference[13].

The current focus is on finding molecules with required properties and finding ways to get reliable and reproducible contacts by major improvements in device fabrications methods. Among different organic molecules there are porphyrins, fluorene and fluorenone as the following explanation.

Structure of Porphyrin:

Porphyrins are an attractive class of organic molecules to investigate for molecular electronic functions[14,15]. The porphyrin molecule consists of four pyrrole cores (the inner ring π-system), and is an attractive building block for molecular-scale devices, because it is highly-conjugated, has a rigid planner geometry and is chemically stable[16,17]. Therefore, we can use it as a basis for wires, switches, transistors and photodiodes[18–20]. Porphyrins can be metalled at the centre by suitable metal ions such as Zn, Fe, Ni, and Co etc, forming metallo-porphyrins[21–23], whereas porphyrin in which no metal is inserted in is called a free-base porphyrin.

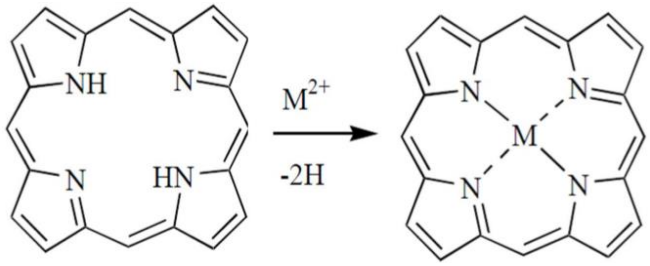

Scheme formation of metallo-porphyrins, M is the incorporated metal atom

Metallo-porphyrins in association with protein globules performs several important biochemical functions in nature where they are founding in haemoglobin, myoglobin, chlorophyll, cytochromes, catalase and paroxidases[24–26]. Interest in metallo-porphyrins is not confined only to the biological field as these compounds are equally important from the chemical, industrial and technological point of view. During the last three decades synthetic porphyrins have been widely studied for various applications spanning a wide range of chemical and biological fields[27–29].

Structure of Fluorene:

Fluorene is a polycyclic aromatic hydrocarbon that has three rings covalently bonded together. The term 'polycyclic' simply means multiple rings are involved. 'Aromatic' means that the compound contains an alternating network of double and single bonds all the way around each benzene ring, which tells us that there are benzene rings present, and 'hydrocarbon' simply means that the molecule contains only carbon and hydrogen atoms. Structurally, it is a five-carbon ring with a benzene ring on each side.

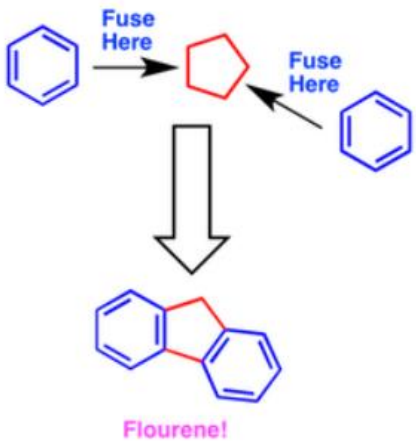

Structure of fluorene

Structure of Fluorenone

Fluorenone is an aromatic compound that contains a five-membered ring with a carbonyl group attached and two benzene rings fused on either side.

Notice that the five-membered ring that looks like a pentagon is sandwiched right in the middle of each benzene ring. These types of ring systems that are joined together like that are called **fused** ring systems. We could say that the five-membered ring has a benzene ring 'fused' to each side of it. A carbonyl group in organic chemistry is always defined as a carbon-oxygen double bond.

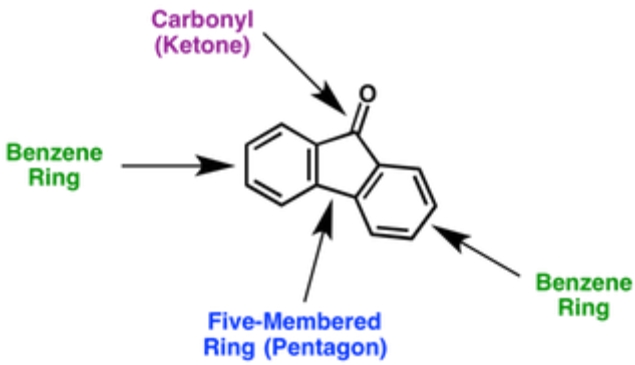

General structure of fluorenone

Due to the presence of an oxygen molecule, the chemical compound in fluorenone give an electrostatic gate between the bonded carbon and oxygen which present fluorenone is more negative than fluorene.

1.2 Thesis outline

Following this chapter, the overview of the thesis as follows:

In the second chapter I will present a simple description of retarded Green's functions. First, I consider a perfect one-dimensional tight binding chain, and then I break the periodicity at a single connection and show how the Green's function is related to the transmission coefficient through the scattering region. Then I will introduce a more general method to calculate the transmission coefficient from the wave function starting with the Schrodinger equation. Finally, I will then show the main features of transport curve through single molecules and briefly discuss about different kinds of resonances, which are: Breit−Wigner resonances, anti-resonances and Fano resonances.

In the third chapter, I will introduce the analytical formula of Wigner delay time starting with the time dependent Schrodinger equation and by applying it to a scattering problem. Then, I will relate this concept to the connectivities to investigate Wigner delay time in graphene-like molecules using tight-binding calculations when the coupling to the molecule is very weak and the Fermi energy coincides with the center of the HOMO-LUMO gap. I will then present and discuss my results related to the Wigner delay time.

In the fourth chapter, I have examined two families of porphyrin oligomers, one with moderate inter-porphyrin coupling, and the other with strong coupling. In moderately-coupled butadiyne-linked wires, the conductance decays exponentially over a wide range

of bias voltages. In contrast, for the series with strong coupling, the conductance increases with length.

In the fifth chapter, I will study the conductance of a family of eight fluorene and fluorenone molecules with *para*/*meta* connectivity and thiol/pyridyl anchor groups. The results reveal that the conductance of these molecules is similar for *para* connectivity, whereas for *meta* connectivity the conductance of fluorene << fluorenone.

Chapter six is the last chapter. It will contain a summary and conclusion of this work and the possible applications that could arise from this work in future.

Bibliography

(1) Lambert, C. J. Basic Concepts of Quantum Interference and Electron Transport in Single-Molecule Electronics. *Chem. Soc. Rev.* **2015**, *44* (4), 875–888.

(2) Sadeghi, H.; Mol, J. a; Lau, C. S.; Briggs, G. A. D.; Warner, J.; Lambert, C. J. Conductance Enlargement in Picoscale Electroburnt Graphene Nanojunctions. *Proc. Natl.Acad.Sci.USA* **2015**, *112* (9), 2658–2663

(3) Elke, S.; Carlos, C. J. *Molecular Electronics: An Introduction to Theory and Experiment*; World Scientific, 2017; Vol. 15.

(4) Scheer, E. Visions for a Molecular Future. *Nat. Nanotechnol.* **2013**, *8* (6), 386.

(5) Li, J.-C.; Wu, J.-Z.; Gong, X. Conductance Switching and Photovoltaic Effect of Ru (II) Complex Molecular Junctions: Role of Complex Properties and the Metal/Molecule Interface. *J. Phys. Chem. Lett.* **2014**, *5* (6), 1017–1021.

(6) Sadeghi, H. Theory of Electron, Phonon and Spin Transport in Nanoscale Quantum Devices. *Nanotechnology* **2018**.

(7) Sakamoto, R.; Katagiri, S.; Maeda, H.; Nishihara, H. Bis (Terpyridine) Metal Complex Wires: Excellent Long-Range Electron Transfer Ability and Controllable Intrawire Redox Conduction on Silicon Electrode. *Coord. Chem. Rev.* **2013**, *257* (9–10), 1493–1506.

(8) Love, J. C.; Estroff, L. A.; Kriebel, J. K.; Nuzzo, R. G.; Whitesides, G. M. Self-Assembled Monolayers of Thiolates on Metals as a Form of Nanotechnology. *Chem. Rev.* **2005**, *105* (4), 1103–1170.

(9) Aradhya, S. V; Venkataraman, L. Single-Molecule Junctions beyond Electronic

Transport. *Nat. Nanotechnol.* **2013**, *8* (6), 399.

(10) Sangtarash, S.; Huang, C.; Sadeghi, H.; Sorohhov, G.; Hauser, J.; Wandlowski, T.; Hong, W.; Decurtins, S.; Liu, S.-X.; Lambert, C. J. Searching the Hearts of Graphene-like Molecules for Simplicity, Sensitivity, and Logic. *J. Am. Chem. Soc.* **2015**, *137* (35), 11425–11431.

(11) Sadeghi, H.; Algaragholy, L.; Pope, T.; Bailey, S.; Visontai, D.; Manrique, D.; Ferrer, J.; Garcia-Suarez, V.; Sangtarash, S.; Lambert, C. J. Graphene Sculpturene Nanopores for DNA Nucleobase Sensing. *J. Phys. Chem. B* **2014**, *118* (24), 6908–6914.

(12) Themistoklis, P. C. T.; Chua, L. Two Centuries of Memristors. *Nat. Mater.* **2012**, *11*, 478–481.

(13) Geng, Y.; Sangtarash, S.; Huang, C.; Sadeghi, H.; Fu, Y.; Hong, W.; Wandlowski, T.; Decurtins, S.; Lambert, C. J.; Liu, S.-X. Magic Ratios for Connectivity-Driven Electrical Conductance of Graphene-like Molecules. *J. Am. Chem. Soc.* **2015**, *137* (13), 4469–4476.

(14) Sadeghi, H.; Sangtarash, S.; Lambert, C. J. Electron and Heat Transport in Porphyrin-Based Singlemolecule Transistors with Electro-Burnt Graphene Electrodes. *Beilstein J. Nanotechnol.* **2015**, *6* (1), 1413–1420. https://doi.org/10.3762/bjnano.6.146.

(15) Noori, M. Quantum Theory of Electron Transport Through Photo-Synthetic Porphyrins, Lancaster University, 2017.

(16) Auwärter, W.; Écija, D.; Klappenberger, F.; Barth, J. V. Porphyrins at Interfaces. *Nat. Chem.* **2015**, *7* (2), 105.

(17) Jurow, M.; Schuckman, A. E.; Batteas, J. D.; Drain, C. M. Porphyrins as Molecular Electronic Components of Functional Devices. *Coord. Chem. Rev.* **2010**, *254* (19–20), 2297–2310.

(18) Sedghi, G.; Sawada, K.; Esdaile, L. J.; Hoffmann, M.; Anderson, H. L.; Bethell, D.; Haiss, W.; Higgins, S. J.; Nichols, R. J. Single Molecule Conductance of Porphyrin Wires with Ultralow Attenuation. *J. Am. Chem. Soc.* **2008**, *130* (27), 8582–8583.

(19) Sena, A. M. P.; Brázdová, V.; Bowler, D. R. Density Functional Theory Study of the Iron-Based Porphyrin Haem (b) on the Si (111): H Surface. *Phys. Rev. B* **2009**, *79* (24), 245404.

(20) Cho, S.; Yoon, M.-C.; Kim, K. S.; Kim, P.; Kim, D. Electron Delocalization in Various Triply Linked Zinc (II) Porphyrin Arrays: Role of Antiaromatic Junctions between Aromatic Porphyrins. *Phys. Chem. Chem. Phys.* **2011**, *13* (36), 16175–16181.

(21) Hoard, J. L. Stereochemistry of Hemes and Other Metalloporphyrins. *Science (80-.).* **1971**, *174* (4016), 1295–1302.

(22) Kaim, W.; Schwederski, B. Katalyse Durch Hämoproteine: Elektronenübertragung, Sauerstoffaktivierung Und Metabolismus Anorganischer Zwischenprodukte. In *Bioanorganische Chemie*; Springer, 2005; pp 114–135.

(23) Noori, M.; Sadeghi, H.; Al-Galiby, Q.; Bailey, S. W. D.; Lambert, C. J. High Cross-Plane Thermoelectric Performance of Metallo-Porphyrin Molecular Junctions. *Phys. Chem. Chem. Phys.* **2017**, *19* (26), 17356–17359.

(24) Smith, E. L. *Principles of Biochemistry: General Aspects*; McGraw-Hill, 1983; Vol. 1.

(25) Huheey, J. E. RL Keiter Inorganic Chemistry. HarperCollins College Publisher 1993.

(26) Outlook, A. G. Porphyrins and Metalloporphyrins: A General Outlook.

(27) Marzilli, L. G. Medical Aspects of DNA-Porphyrin Interactions. *New J. Chem.* **1990**, *14*, 409–420.

(28) Meunier, B. Metalloporphyrins as Versatile Catalysts for Oxidation Reactions and Oxidative DNA Cleavage. *Chem. Rev.* **1992**, *92* (6), 1411–1456.

(29) Mukundan, N. E.; Petho, G.; Dixon, D. W.; Marzilli, L. G. DNA-Tentacle Porphyrin Interactions: AT over GC Selectivity Exhibited by an Outside Binding Self-Stacking Porphyrin. *Inorg. Chem.* **1995**, *34* (14), 3677–3687.

Chapter 2

Theory of single particle transport

2.1. Introduction

The theory of single particle transport is introduced as the main numerical tool for studying a range of molecular geometrics and involves detailed investigation of electronic properties. Molecular electronics is focused on understanding the electrical properties of molecular junctions where a molecule is attached between electrodes and the ballistic transport is occurring through energy levels of the molecules. The coupling strength existing between lead and molecules is considered to be small in comparison to intra- electrode and inter molecular binding strengths. One of the important challenges in molecular electronic is how to connect the molecule to metallic or any other electrodes to probe its electronic properties. A scattering process is also involved in the movement from electrode to molecule and then from molecule to electrode. The scattering process from electrode junction and molecular bridge can be understood by following a general approach of the Green's function formalism which helps to achieve this process. In the beginning of this chapter the discussion will start with a brief derivation of the Landauer formula then I will introduce a simple formula of a retarded Green's function which has been explained for a one-dimensional tight binding chain. By breaking the periodicity of this lattice at a single connection it is seen that, the Green's function is directly related to transmission coefficient through the scattering region.

Then, to determine the behaviour of resonance for the transmission coefficient as a function of energy I introduce the Breit-Wigner formula and Fano- anti resonance phenomena which is an important concept that is related to electrons transmission behaviour. These phenomena explain the resulting changes in transmission coefficient by varying energy level.

2.2. The Landauer Formula

The Landauer formula[1,2] is the standard way to describe transport phenomena in ballistic mesoscopic systems and is applicable for phase coherent systems, where a single wave function is sufficient to describe the electronic flow. The final result is a formula which relates the conductance of system to the S-matrix of a scattering region attached to two semi-infinite leads.

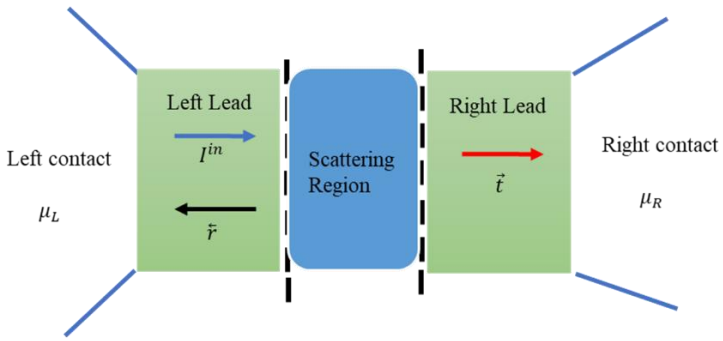

Figure 2.2.1: A mesoscopic scatterer connected to contacts by ballistic leads. Where the chemical potential in the contacts is μ_L (left) and μ_R (right) respectively.

To understand the main ideas behind this formula I start by considering a mesoscopic scatterer connected to two contacts, which behave as electron reservoirs, forming two ideal ballistic leads (Figure 2.2.1). All inelastic relaxation processes are limited to the

reservoirs[3]. The reservoirs have slightly different chemical potentials $\mu_L > \mu_R \Longrightarrow \mu_L\text{-}\mu_R = e\delta V > 0$, which will drive electrons from the left to the right reservoir. For one open channel the zero-temperature incident electric current (δI^{in}) generated by the chemical potential difference:

$$\delta I = ev\left(\frac{\partial n}{\partial E}\right)(\mu_L\text{-}\mu_R) \qquad (2.2.1)$$

here, e is the electronic charge, vg is the group velocity and $\partial n/\partial E$ is the density of states (DOS).

the system is considered as one dimensional, then we can write:

$$\frac{\partial n}{\partial E} = \frac{\partial n}{\partial k}\frac{\partial k}{\partial E} = \frac{\partial n}{\partial k}\frac{1}{v\hbar} \qquad (2.2.2)$$

As in one-dimension, $\frac{\partial n}{\partial k} = \frac{1}{\pi}$ and $\frac{\partial n}{\partial E} = \frac{1}{vh}$, since the group velocity is $v = \frac{1}{\hbar}\frac{dE}{dk}$, by this and after including a factor 2 for spin, equation (2.2.1) will be:

$$\delta I = \frac{2e}{h}(\mu_L\text{-}\mu_R) = \frac{2e^2}{h}\delta V \qquad (2.2.3)$$

Where δV is the voltage which corresponding to the chemical potential difference. In the absence of a scattering region it is clear that from equation (2.2.3), the conductance for one open channel is $(\frac{e^2}{h})$, which is around 77.5 μS, or the resistance $(\frac{h}{e^2})$ about 12.9 kΩ. By considering a scattering region in the system, the current is partially reflected with a probability $R = |r|^2$ and partially transmitted with a probability $T = |t|^2$. The current passing through the scatterer to the right lead will be:

$$\delta I = \frac{2e^2}{h}T\delta V \Rightarrow \frac{\delta I}{\delta V} = G = \frac{2e^2}{h}T \qquad (2.2.4)$$

This equation is the Landauer formula, were the conductance $G = \frac{I}{V} = \left(\frac{2e^2}{h}\right)T$. And the transmission is evaluated at the Fermi energy[4]

The Landauer formula has been generalized for the case of more than one open channel by Buttiker[2]. In this case the transmission coefficient is replaced by the sum of all the transmission amplitudes describing electrons incoming from the left contact and arriving to the right contact. The Landauer formula equation (2.2.4) for many open channels becomes:

$$\frac{\delta I}{\delta V} = G = \frac{2e^2}{h}\sum_{i,j}\left|t_{i,j}\right|^2 = \frac{2e^2}{h}\mathrm{Trace}(tt^{\dagger}) \qquad (2.2.5)$$

Where, $t_{i,j}$ here is the amplitude of transmission describing scattering from the jth channel of the left lead to i^{th} channel of the right lead and G is the electrical conductance and $r_{i,j}$ is the reflection amplitudes which describe the electron passing through scattering region in the opposite direction. By combining the amplitudes of transmission and reflection, can be define the scattering S matrix which involves the electron coming from the left lead and the right lead as follow:

$$S = \begin{pmatrix} r & t' \\ t & r' \end{pmatrix} \qquad (2.2.6)$$

Here, r and t represent the electrons coming from the left, also r' and t' describe electrons coming from the right. In equation (2.2.6) r, t, r' and t' are complex matrices for more than one open channel, and due to charge conservation satisfy $SS^{+} = I$.

2.3. Theory of electron transport

To have a good understanding of electron transport we should know about the transmission probability (*T*) which is related to the conductance G at the Fermi energy *E* by the Landauer formula[5,6]

$$G(E) = G_o T(E) \tag{2.3.1}$$

Where the electrical conductance is *G(E)* as a function of energy and the quantum conductance is represented by $G_o = \frac{2e^2}{h}$ where 'e' is the electron charge, h is the Planck's constant. *T (E)* has denotes the transmission coefficient as a function of energy, and is the probability that an electron with energy *E* can transfer from one electrode to the other.

This leads us to the scattering formalism shown schematically below:

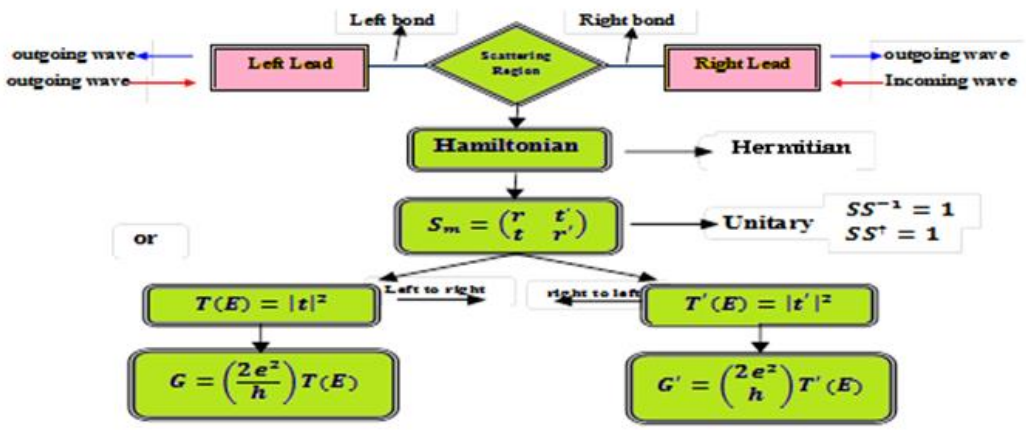

Diagram 2.3.1: has shown the transport mechanism where it is combination of mathematical and physical structures. The transport mechanism is composed of two types of probabilities as probability of *R (E)* and probability of *T(E).*

$$|t|^2 + |r|^2 = 1 \;\; \rightarrow T(E) + R(E) = 1$$

2.4. Scattering Theory

2.4.1 One dimensional (1-D) linear crystalline lattice

To give a clear outline of the methodology used, it is helpful to calculate the scattering matrix for a simple one-dimensional structure before representing a generalized methodology. We use the Green's function approach for the derivation and in this section, I am going to consider a simple tight-binding model in periodic systems to get a qualitative understanding of electronic structure calculation having on-site energies (ε_o) along with hopping elements($-\gamma$) as shown in figure (2.4.1).

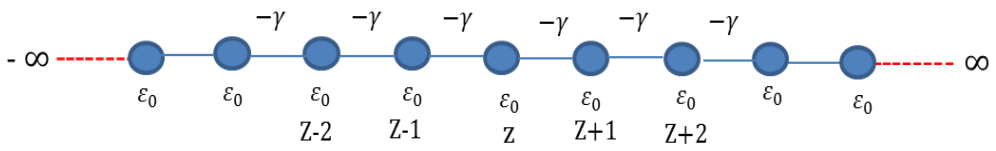

Figure 2.4.1: Tight-binding model of a one-dimensional periodic lattice with energy site ε_o and hopping elements($-\gamma$) where Z is the label of the orbital.

The matrix form of the Hamiltonian is written simply:

$$H = \begin{pmatrix} \ddots & -\gamma & & \\ -\gamma & \varepsilon_o & -\gamma & \\ & -\gamma & \varepsilon_o & -\gamma \\ & & -\gamma & \ddots \end{pmatrix}$$

For obtaining z row of Hamiltonian the Schrodinger equation is represented as;

$$-\gamma\Psi_{(z-1)} + (-E + \varepsilon_o)\Psi_{(z)} - \gamma\Psi_{(z+1)} = 0 \qquad (2.4.1)$$

For any function $\Psi_{(z)}$ that has to be a wave function, it only needs to satisfy criteria of the Schrodinger equation (2.4.1)

It is assumed that $\gamma = \gamma^*$ then by substituting a plane wave into equation (2.4.1) leads to the dispersion relation (2.4.2).

$$E = \varepsilon_o - 2\gamma \cos k \tag{2.4.2}$$

The wave number is commonly represented by the quantum number (k) and the wave function is linked to the retarded Greens function represented as $g(z, z')$. This equation is very similar to the Schrödinger equation.

$$\left.\begin{aligned} (E-H)\, g(z, z') &= \delta_{(z,z')} \\ -\gamma g(z-1, z') + (E-\varepsilon_o)\, g(z, z') - \gamma\, g(z+1, z') &= \delta_{(z,z')} \end{aligned}\right\} \tag{2.4.3}$$

Where

$$\delta_{(z,z')} = 1, \qquad \text{if } z = z'$$

And

$$\delta_{(z,z')} = 0, \qquad \text{if } z \neq z'$$

The Green's function $g(z, z')$ of a system is defined to be the amplitude at the point z, resulting from an excitation at point z'. Two waves will be generated as a result of this excitation and the waves moves outwards from the excitation points. The figure (2.4.2) represents the amplitudes B and D.

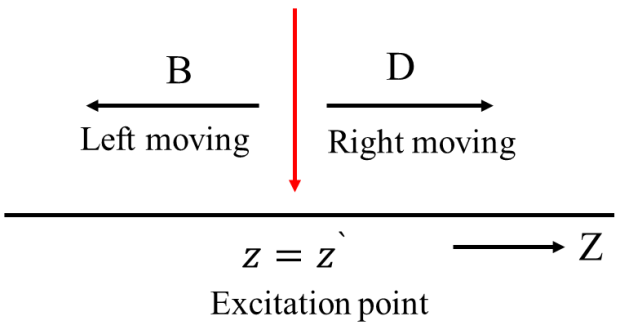

Figure 2.4.2: Structure of retarded Green's function having an infinite one- dimensional lattice. The wave is propagated towards the left and right sides through excitation at $z = z'$ with amplitude B and D respectively.

We expect two waves traveling outward from the excitation point with amplitude B and D as represented in figure (2.4.2). These waves can be simply expressed as:

$$g(z, z') = \begin{cases} De^{ikz}, & z \geq z' \\ Be^{-ikz}, & z \leq z' \end{cases} \tag{2.4.4}$$

This expression satisfies equation (2.4.3) at every point, where the condition $z = z'$ is not satisfied where the Green's function must be continuous at $z = z'$.

$$[g(z, z')]_{Left} = [g(z, z')]_{Right} \tag{2.4.5}$$

$$Be^{-ikz'} = De^{ikz'} \tag{2.4.6}$$

$$B = De^{2ikz'} \tag{2.4.7}$$

So, we find that,

$$g(z, z') = \begin{cases} D\, e^{ikz} = D\, e^{ikz'}\, e^{ik(z-z')} & z \geq z' \\ De^{2ikz'} e^{-ikz} = De^{ikz'} e^{ik(z'-z)} = D\, e^{ikz'}\, e^{ik(z'-z)} & z \leq z' \end{cases} \tag{2.4.8}$$

We know that, the power of the complex exponent has to be always positive and the simplified form of latter equation is represented as;

$$g(z,z') = De^{ikz'}e^{ik|z'-z|}, \qquad (2.4.9)$$

Secondly, this expression must satisfy the Green's equation, $(E-H)g(z,z') = \delta_{z,z'}$:

$$\delta_{z,z'} = Eg(z,z')-\varepsilon_0 g(z-z') + \gamma g(z+1,z') + \gamma g(z-1,z') \qquad (2.4.10)$$

We find the solution at $z = z'$:

$$1 = (E-\varepsilon_0)g(z,z) + \gamma g(z+1,z) + \gamma g(z-1,z)$$

$$= D\, e^{ikz'}[(E-\varepsilon_0)e^{ik|z-z|} + \gamma e^{ik|z+1\, z|} + \gamma e^{ik|z-1\, z|}] \qquad (2.4.11)$$

We solve for $D\, e^{ikz'}$:

$$\frac{1}{D\, e^{ikz'}} = (E-\varepsilon_0) + \gamma e^{ik} + \gamma e^{ik}$$

$$= (E-\varepsilon_0) + \gamma e^{ik} + \gamma e^{ik} + \gamma e^{-ik} - \gamma e^{-ik}$$

$$= \gamma e^{ik} - \gamma e^{-ik}$$

$$D\, e^{ikz'} = \frac{1}{2i\gamma \sin k} \qquad (2.4.12)$$

Since we know that from the Schrödinger equation, the group velocity $hv_g = 2\gamma \sin k$ we find that, the Green's function for a one-dimensional chain can be written as:

$$g^R(z,z') = \frac{1}{ihv_g}\, e^{ik|z-z'|} \qquad (2.4.13)$$

There are more solutions that can be found for this problem in the literature[3,7,8]. In above equation, I have solved for the retarded Green's function $g^R(z,z')$, but the advanced Green's function $g^A(z,z')$ is an equally valid solution;

$$g^A(z,z') = \frac{-1}{i\hbar v_g}\, e^{-ik|z-z'|} = \frac{i}{\hbar v_g}\, e^{-ik|z-z'|} \qquad (2.4.14)$$

The retarded Green's function describes outgoing waves from an excitation point ($z = z'$), but the advanced Greens' function is describing two incoming waves that vanish at the excitation point. From here I will use the retarded Green's function and for the sake of simplicity, drop the R from its representation. So $g(z, z') = g^R(z, z')$.

2.4.2 Semi-infinite one-dimensional lattice

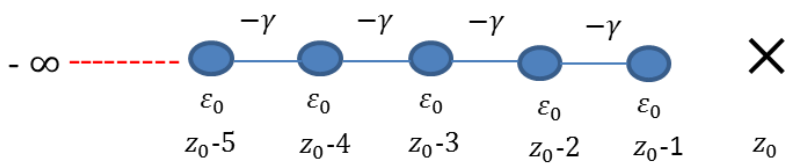

Figure 2.4.3: Tight-binding model of a semi-infinite one-dimensional lattice with energy site ε_o and hopping elements($-\gamma$).

To satisfy the boundary condition, we introduce another plane wave component with a new amplitude:

$$g(z, z') = \frac{1}{ihv_g} e^{ik|z-z'|} + A\, e^{-ik|z-z'|} \qquad (2.4.15)$$

From the condition $g(z, z_0) = 0$, $z \leq z'$, we find:

$$g(z, z_0) = \frac{1}{ihv_g} e^{ik(z_0-z)} + A\, e^{-ik(z_0-z)}$$

$$A = -\frac{1}{ihv_g} e^{2ik(z_0-z)} \qquad (2.4.16)$$

By substituting this back into the Green's function, we find:

$$g(z, z') = \frac{1}{ihv_g} e^{ik(z'-z)} - \frac{1}{ihv_g} e^{2ik(z_0-z)}\, e^{-ik(z'-z)}$$

$$g(z,z') = \frac{1}{ihv_g}\left[e^{ik(z'-z)} - e^{ik(2z_0-z-z')}\right] \qquad (2.4.17)$$

The second condition is that, any point beyond z_0-1 does not have effect from a source in the chain. So, if $z \geq z'$and $z = z_0$, we expect $g(z_0, z) = 0$ so from this condition, we find:

$$g(z_0,z) = \frac{1}{ihv_g} e^{ik(z_0-z')} + A\, e^{-ik(z_0-z')}$$

$$A = -\frac{1}{ihv_g} e^{2ik(z_0-z')} \qquad (2.4.18)$$

By substituting this back into the Green's function, we find:

$$g(z,z') = \frac{1}{ihv_g} e^{ik(z-z')} - \frac{1}{ihv_g} e^{2ik(z_0-z')}\, e^{-ik(z-z')}$$

$$g(z,z') = \frac{1}{ihv_g}\left[e^{ik(z-z')} - e^{ik(2z_0-z-z')}\right] \qquad (2.4.19)$$

By summarizing these two results we find:

$$\begin{cases} \frac{1}{ihv_g}\left[e^{ik(z-z')} - e^{ik(2z_0-z-z')}\right], & z \geq z' \\ \frac{1}{ihv_g}\left[e^{ik(z'-z)} - e^{ik(2z_0-z-z')}\right], & z \leq z' \end{cases} \qquad (2\ .4.20)$$

The above result can be written as:

$$g(z,z') = \frac{1}{ihv_g}\left[e^{ik|z-z'|} - e^{ik(2z_0-z-z')}\right] = g^{\infty}_{z,z'} + \Psi^{z_0}_{z,z'} \qquad (2.4.21)$$

2.4.3 One dimensional (1-D) scattering

As an example of the above, the surface Green's function is evaluated with the site $z = z_0\text{-}1$. So, the surface Green's function is:

$$g(z_0\text{-}1,\ z_0\text{-}1) = \frac{1}{ihv_g}\left[\, e^{ik|z_0\text{-}1\text{-}z_0+1|} - e^{ik(2z_0\text{-}z_0+1\text{-}z_0+1)}\right] \qquad (2.4.22)$$

This leads to the simple form;

$$g(z_0\text{-}1,\ z_0\text{-}1) = \frac{1}{ihv_g}(\text{-}2i\sin k)\, e^{ik} \qquad (2.4.23)$$

$$g(z_0\text{-}1,\ z_0\text{-}1) = -\frac{2i\sin k}{2i\gamma\sin k}\, e^{ik} = -\frac{e^{ik}}{\gamma} \qquad (2.4.24)$$

2.4.4 One-dimensional (1-D) Scattering Using Green's functions

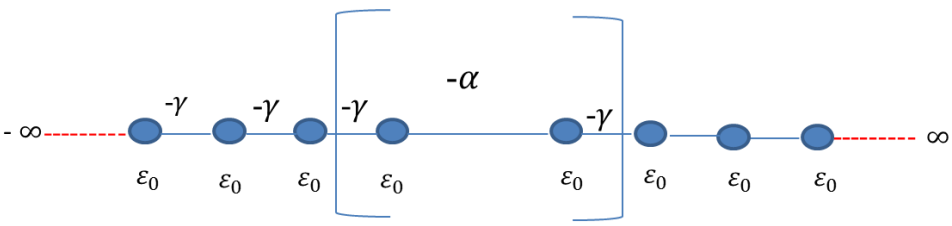

Figure 2.4.4: Tight binding model of two semi-infinite leads with one site energies ε_0 and couplings $-\gamma$, coupled by hopping element $-\alpha$.

We consider two semi-infinite one-dimensional leads both leads are equal with ε_0 on-site potential and $-\gamma$ hopping elements. The total Green's function is obtained in the case of decoupled leads ($\alpha = 0$)and it is represented by;

$$g = \begin{pmatrix} -\frac{e^{ik}}{\gamma} & 0 \\ 0 & -\frac{e^{ik}}{\gamma} \end{pmatrix} = \begin{pmatrix} g_L & 0 \\ 0 & g_R \end{pmatrix} \qquad (2.4.25)$$

This Green's function represents two decoupled semi-infinite leads, $g = (E\text{-}h_1)^{-1}$ where h_1 is the Hamiltonian of two decoupled semi-infinite leads and we have created an infinite matrix for defining this Hamiltonian as;

$$h_1 = \begin{pmatrix} \ddots & \ddots & 0 & 0 & 0 & 0 & 0 & 0 \\ \ddots & \ddots & -\gamma & 0 & 0 & 0 & 0 & 0 \\ 0 & -\gamma\varepsilon_o & -\gamma & 0 & 0 & 0 & 0 & 0 \\ 0 & 0 & -\gamma\varepsilon_o & -\gamma & 0 & 0 & 0 & 0 \\ 0 & 0 & 0 & -\gamma\varepsilon_o & -\gamma & 0 & 0 & 0 \\ 0 & 0 & 0 & 0 & -\gamma\varepsilon_o & -\gamma & 0 & 0 \\ 0 & 0 & 0 & 0 & 0 & -\gamma & \ddots & \ddots \\ 0 & 0 & 0 & 0 & 0 & 0 & \ddots & \ddots \end{pmatrix} \tag{2.4.26}$$

We can connect the two leads by a hopping element, and the Hamiltonian for whole system or coupled system in figure (2.2.4) becomes $H = h_1 + h_0$ where h_0 contains the coupling parameters

$$h_0 = \begin{pmatrix} 0 & \alpha \\ \alpha & 0 \end{pmatrix} \tag{2.4.27}$$

The Green's function obtained for coupled system will be found by using Dyson's equation as follows;

$$G = (E\text{-}H)^{-1} = (E\text{-}\ h_1\text{-}h_0)^{-1} \tag{2.4.28}$$

$$G = (g^{-1}\text{-}h_0)^{-1} \tag{2.4.29}$$

The solution, in this case, will be:

$$G = \left(\begin{pmatrix} -\frac{e^{ik}}{\gamma} & 0 \\ 0 & -\frac{e^{ik}}{\gamma} \end{pmatrix}^{-1} - \begin{pmatrix} 0 & \alpha \\ \alpha & 0 \end{pmatrix} \right)^{-1} \tag{2.4.30}$$

$$G = \frac{1}{\gamma^2 e^{-2ik} - \alpha^2} \begin{pmatrix} -\gamma e^{-ik} & \alpha \\ \alpha^* & -\gamma e^{-ik} \end{pmatrix} \tag{2.4.31}$$

In order to calculate transmission $\vec{t}$ and reflection $\overleftarrow{r}$ amplitudes, we use the Greens' function presented in equation (2.4.31) and apply them to the Fisher Lee relation which calculates the scattering amplitudes of the scattering problem by relating it to the Green's function of the same problem[5,7].

Since we know the Green's function components from equation (2.4.31), we can define the transmission and reflection coefficients. When the source from the excitation point sends two waves travelling outwards, one away from the scatter and one towards the scatter with amplitude B and D respectively. So, the Green's function contains information about two waves: a left wave or a reflected wave ($D\, e^{-ik|z-z'|} + Bre^{ik|z-z'|}$) and the transmitted right wave ($Bte^{ik|z-z'|}$)). Here we use symbol $\overleftarrow{t}$ for transmitted right wave and $\vec{r}$ for reflected left wave where arrows are pointing directions of amplitudes.

$$1 + r = -ihv_g \frac{\gamma\, e^{-ik}}{\gamma^2 e^{-2ik} - \alpha^2} \qquad (2.4.32)$$

$$t = ihv_g \frac{\alpha\, e^{ik}}{\gamma^2 e^{-2ik} - \alpha^2} \qquad (2.4.33)$$

To calculate the transmission and reflection probabilities we use these coefficients as follows;

$$T = |t|^2 \qquad \text{and} \qquad R = |r|^2$$

So, by using the Landauer formula represented in equation (2.3.1) we can also calculate the conductance of the system.

2.5. More general method to calculate the transmission from a wave function

In this section I discuss the relationship between a wave function and Green's function in more details and present a more general method for computing the transmission amplitude of an arbitrary scattering region connected to one-dimensional leads.

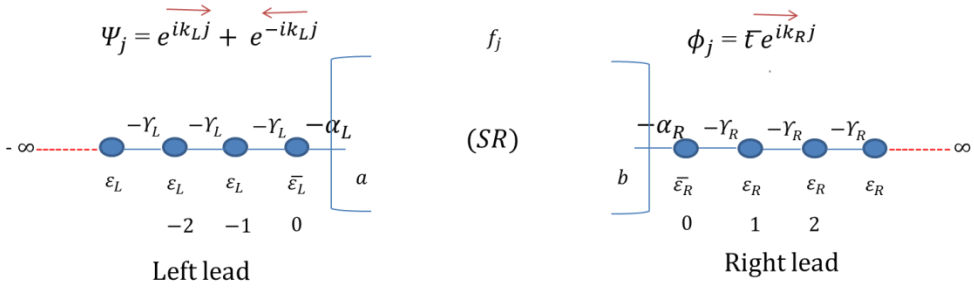

Figure 2.5.1: Simple tight binding model having two different infinite leads that are connected with independent scattering regions via hoping elements ($-\alpha_L$) and ($-\alpha_R$).

The structure presented in figure (2.5.1) can be described in detail to provide a clear picture of the methodology used. We have two different leads one of them called the left lead and another one the right lead. The left lead is a one-dimensional periodic lattice constructed with site energies ε_L and coupling $-\gamma_L$ and in the same for the right lead just the values of the site energies are ε_R and the coupling $-\gamma_R$. The hopping elements $-\alpha_L$ and $-\alpha_R$ are used for connecting the infinite leads with independent scattering regions. In this section, I will use the form of Green's function to solve the problem and calculate the transmission coefficient as a function of energy.

2.5.1 Schrödinger equation representation

The problem is solved by considering the Schrödinger equation for the current system. The equation is represented below:

$$H|\Psi\rangle = E|\Psi\rangle \tag{2.5.1}$$

The Hamiltonian of the scattering region is represented by H that will be used for describing the current system. The eigenvalues are represented by E of the Hamiltonian H and Ψ_j are used to present the wave function of the whole system and developing the equation.

$$H\begin{pmatrix} \vdots \\ \Psi_{-2} \\ \Psi_{-1} \\ \Psi_0 \\ f_a \\ \vdots \\ f_b \\ \phi_0 \\ \phi_1 \\ \phi_2 \\ \vdots \end{pmatrix} = E\begin{pmatrix} \vdots \\ \Psi_{-2} \\ \Psi_{-1} \\ \Psi_0 \\ f_a \\ \vdots \\ f_b \\ \phi_0 \\ \phi_1 \\ \phi_2 \\ \vdots \end{pmatrix} \tag{2.5.2}$$

The Schrödinger equation is written as;

$$\bar{\varepsilon}_L\Psi_0 - \gamma_L\Psi_{-1} - \alpha_L f_a = E\,\Psi_0 \tag{2.5.3}$$

$$\bar{\varepsilon}_R\phi_0 - \gamma_R\phi_{+1} - \alpha_R f_b = E\phi_0 \tag{2.5.4}$$

$$\therefore(\bar{\varepsilon}_L - \varepsilon_L)\Psi_0 + \gamma_L\Psi_1 = \alpha_L f_a \tag{2.5.5}$$

$$(\bar{\varepsilon}_R - \varepsilon_R)\phi_0 + \gamma_R\phi_{-1} = \alpha_R f_b \tag{2.5.6}$$

Since

$$\Psi_1 = e^{ik} + re^{-ik}$$

and

$$\Psi_0 = 1 + r$$

we obtain

$$\Psi_1 = 2i \sin k_L + \Psi_0 e^{-ik_L} \tag{2.5.7}$$

where

$$\phi_{-1} = \phi_0 e^{-ik_R} \qquad \text{and} \qquad \phi_0 = \bar{t}$$

So,

$$t = \left(\frac{v_R}{v_L}\right)^{\frac{1}{2}} \times \bar{t} \tag{2.5.8}$$

So, our aim here is to write Ψ_1 and ϕ_{-1} in terms of Ψ_0 and ϕ_0 to make the problem easier where ($\vec{t}$) is the transmission amplitude and ($\overleftarrow{r}$) is the reflection amplitude.

An appropriate boundary condition has been introduced in order to derive the Green's function for an infinite lead and the system will be represented as;

$$f_a = \frac{\gamma_L}{\alpha_L} \Psi_1 \tag{2.5.9}$$

$$f_b = \frac{\gamma_R}{\alpha_R} \phi_{-1} \tag{2.5.10}$$

Hence; we know that from the general Schrödinger equation:

$$H|f_j\rangle = E|f_j\rangle + |S\rangle \tag{2.5.11}$$

Also,

$$\sum_{j=1}^{N} H_{ij} f_j = E f_i + \alpha_L \Psi_0 \delta_i + \alpha_R \phi_0 \delta_i$$

$$(E-H)|f\rangle = -|S\rangle \quad \text{where,} \quad |S\rangle = \begin{pmatrix} 0 \\ 0 \\ \vdots \\ -\alpha_L \Psi_0 \\ 0 \\ 0 \\ \vdots \\ -\alpha_R \phi_0 \\ \vdots \end{pmatrix} \tag{2.5.12}$$

So, the above equation is transformed as:

$$|f\rangle = -\, g(E)\, |S\rangle \qquad (2.5.13)$$

The problem can be solved after calculating the Greens' function of the normal form and it can be written as;

$$g(E) = (E-H)^{-1} \qquad (2.5.14)$$

So,

$$\begin{pmatrix} f_a \\ f_b \end{pmatrix} = -\begin{pmatrix} g_{aa} & g_{ab} \\ g_{ba} & g_{bb} \end{pmatrix} \begin{pmatrix} -\alpha_L \Psi_0 \\ -\alpha_R \phi_0 \end{pmatrix} \qquad (2.5.15)$$

This yields:

$$-\begin{pmatrix} g_{aa}\,\alpha_L + \frac{\gamma_L}{\alpha_L} e^{-ik_L} & g_{ab}\,\alpha_R \\ g_{ba}\,\alpha_L & g_{bb}\,\alpha_R + \frac{\gamma_R}{\alpha_R} e^{-ik_R} \end{pmatrix} \begin{pmatrix} \Psi_0 \\ \phi_0 \end{pmatrix} + \frac{\gamma_L}{\alpha_L}\; 2i \sin k_L \begin{pmatrix} 1 \\ 0 \end{pmatrix} \qquad (2.5.16)$$

We want to calculate the transmission coefficient, which is obtained from ϕ_0.

So,

$$\begin{pmatrix} \Psi_0 \\ \phi_0 \end{pmatrix} = -g^{-1} \times \begin{pmatrix} 1 \\ 0 \end{pmatrix} \frac{\gamma_L}{\alpha_L}\, 2i \sin k_L \qquad (2.5.17)$$

$$\begin{pmatrix} \Psi_0 \\ \phi_0 \end{pmatrix} = \frac{1}{\det g} \begin{pmatrix} g_{bb}\,\alpha_R + \frac{\gamma_R}{\alpha_R} e^{-ik_R} \\ g_{ba}\,\alpha_L \end{pmatrix} \times \frac{\gamma_L}{\alpha_L}\, 2i \sin k_L \qquad (2.5.18)$$

By calculating the determinant of g and we find

$$\det g = \frac{\gamma_L\,\gamma_R}{\alpha_L\,\alpha_R}\, e^{-i(k_L + k_R)} [1 + g_{aa} \frac{\alpha_L{}^2}{\gamma_L} e^{ik_L} + g_{bb} \frac{\alpha_R{}^2}{\gamma_R} e^{ik_R} - (g_{aa}\, g_{bb} - g_{ba}\, g_{ab}) \frac{\alpha_L{}^2\, \alpha_R{}^2}{\gamma_L\, \gamma_R} e^{i(k_L + k_R)} \qquad (2.5.19)$$

So,

$$\phi_0 = \bar{t} = \frac{g_{ba}\alpha_L}{\det g} \times \frac{\gamma_L}{\alpha_L}\, 2i \sin k_L \qquad (2.5.20)$$

Where,

$$\phi_0 = \bar{t}\, \frac{\alpha_L\, \alpha_R}{\gamma_L\, \gamma_R} \times e^{i(k_L + k_R)} \times \frac{g_{ba}}{\det g} \times \gamma_L 2i \sin k_L \qquad (2.5.21)$$

So, by using equation (2.5.8) we obtain:

$$t = \frac{i\,(v_R\, v_L)^{1/2}}{\alpha_L\, \alpha_R} \times \frac{g_{ba}}{\det g} \times e^{i(k_L + k_R)} \qquad (2.5.22)$$

Where $v_L = 2\gamma_L \sin k_L$ is the group velocity of the left lead.

The transmission coefficient T is obtained from

$$T = |t|^2 \qquad (2.5.23)$$

Equations (2.5.22) and (2.5.23) are the most general formula to calculate the transmission probability for any scattering region connected to identical or non-identical leads.

The completely general technique for calculating the Green's function which a scattering matrix *S* and the transport coefficient of a finite super-lattice connected to crystalline semi-infinite leads can be found in[9].

2.6. Features of the Transmission Curve

Transmission resonances associated with quantum interference is the main feature of electron transport through single molecules and phase coherent nanostructures. By looking at the properties of these resonances we can understand the transmission process. Here, I will briefly discuss some different kinds of resonances, which are: Breit−Wigner resonances[10], anti-resonances[11,12] and Fano resonances[13,14].

2.6.1 Breit-Wigner Resonance

In the field of molecular electronics, where the dominant transport mechanism is resonant transport through the energy levels of the molecules, studying of Breit-Wigner formula is very important to understand the behaviour of these resonances for the function *T(E)*[15].To study the resonance line shapes attributed to Breit-Wigner formula, we can

achieve this in our model by making the bonds α and β which couple to the scatterer ε_1 to be very weak the strength of the coupling determines the width of the resonance and the on-site energy its position.

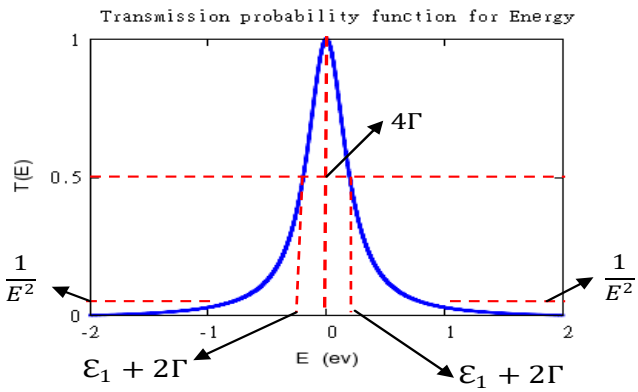

Figure 2.6.1: Shows the shape of resonance by studying of the Breit-Wigner formula a single atom molecule.

In figure (2.6.2) I have presented the one dimensional (1-D) linear chain which contain one impurity ε_1 in the middle of chain that is attached to the left lead by bond α and to the right lead by bond β and γ is the coupling in the leads.

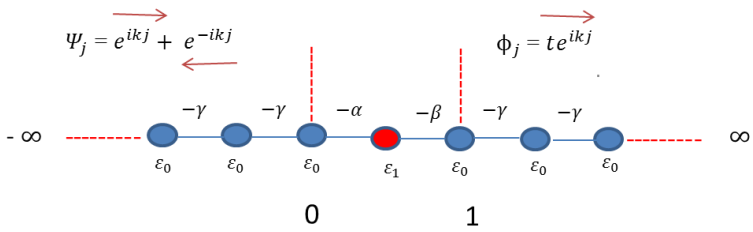

Figure 2.6.2: illustrated one impurity with asymmetric coupling to the two leads.

From the above system we can write that:

$$\Psi_0 = 1+r\,, \qquad \phi_1 = te^{ik} \quad \text{and} \quad |F> = \begin{pmatrix} \vdots \\ \vdots \\ F_{-1} \\ F_0 \\ f \\ F_1 \\ F_2 \\ \vdots \\ \vdots \end{pmatrix}$$

So, when $j \leq 0 \rightarrow F_j = \Psi_j$ and if $j \geq 1 \rightarrow F_j = \phi_j$

j is an impurity position and $F_j = f$

We use Schrodinger equation to solve the problem where we start from j=0 so, we can write it as;

$$\mathcal{E}_0\Psi_o - \gamma\Psi_{-1} - \alpha f = E\Psi_o \tag{2.6.1}$$

$$\mathcal{E}_0\Psi_o - \gamma\Psi_{-1} - \gamma\Psi_1 = E\Psi_o \tag{2.6.2}$$

From these two equations we can find that, $\Psi_1 = \frac{\alpha}{\gamma} f$

For the j=1 position;

$$\mathcal{E}_0\phi_1 - \gamma\phi_2 - \beta f = E\phi_1 \tag{2.6.3}$$

$$\mathcal{E}_0\phi_1 - \gamma\phi_1 - \gamma\phi_0 = E\phi_1 \tag{2.6.4}$$

From these two equations $\phi_1 = \frac{\beta}{\gamma} f$

Now by rewrite Schrodinger equation for an impurity f

$$\mathcal{E}_1 f - \beta\phi_1 - \alpha\Psi_o = Ef \tag{2.6.5}$$

$$(E - \mathcal{E}_1)f = -\beta\phi_1 - \alpha\Psi_o \tag{2.6.6}$$

From figure (2.6.2) we can introduce:

$$\Psi_o = r + 1 \quad , \quad \phi_o = t$$

$$\Psi_{-1} = e^{-ik} + re^{ik} \quad , \quad \phi_1 = te^{ik} = \phi_0 e^{ik}$$

So,

$$\Psi_1 = e^{-ik} + re^{ik} + e^{ik} - e^{ik} = 2isink + \Psi_0 e^{-ik}$$

$$\Psi_1 = 2isink + \Psi_0 e^{-ik} = \frac{\alpha}{\gamma} f$$

$$\phi_0 = \phi_1 e^{-ik} = \frac{\beta}{\gamma} f$$

$$\Psi_0 = e^{ik}(\frac{\alpha}{\gamma} f - 2isink)$$

$$\phi_1 = \frac{\beta}{\gamma} f\, e^{ik}$$

By substituting the value of Ψ_0 and ϕ_1 into equation (2.6.6) we get:

$$\Psi_0 = -\alpha e^{ik}\left(\frac{\alpha}{\gamma} f - 2isink\right) - \beta \frac{\beta}{\gamma} f e^{ik} = (E - \varepsilon_1) f \qquad (2.6.7)$$

$$f[(E - \varepsilon_1) + \frac{\alpha^2}{\gamma} e^{ik} - \frac{\beta^2}{\gamma} e^{ik}] = 2i\gamma sinke^{ik} \qquad (2.6.8)$$

$$f = \frac{2i\gamma sinke^{ik}}{(E - \varepsilon_1) + \left(\frac{\alpha^2}{\gamma} + \frac{\beta^2}{\gamma}\right)(cosk + isink)} \qquad (2.6.9)$$

By assuming; $\Gamma_L = \frac{\alpha^2 sink}{\gamma}$, $\Gamma_R = \frac{\beta^2 sink}{\gamma}$ where $\Gamma = \Gamma_L + \Gamma_R$

$\sigma_L = \frac{\alpha^2 cosk}{\gamma}$, $\sigma_R \ \frac{\beta^2 cosk}{\gamma}$ where $\sigma = \sigma_L + \sigma_R$

$$f = \frac{2i\gamma sinke^{ik}}{(E - (\varepsilon_1 - \sigma)) + i\Gamma} \qquad (2.6.10)$$

Where , $\phi_o = t = \frac{\beta}{\gamma} f$ (2.6.11)

By substituting the value of f into the above equation we get:

$$f = \frac{2i\frac{\alpha^2}{\gamma^2}\beta^2 \sin k e^{ik}}{(E-(\varepsilon_1-\sigma))+i\Gamma} \qquad (2.6.12)$$

The formula for transmission coefficient as a function of energy will be:

$$T(E) = |t|^2 = \frac{4\frac{\alpha^2}{\gamma^2}\beta^2 \sin^2(k) e^{ik}}{(E-(\varepsilon_1-\sigma))^2+(i\Gamma)^2} \qquad (2.6.13)$$

$$T(E) = \frac{4\,\Gamma_L\,\Gamma_R}{(E-(\varepsilon_1-\sigma))^2+\Gamma^2} \qquad (2.6.14)$$

For scattering which is not symmetric : where $\Gamma_L \neq \Gamma_R$

Then the formula on resonance becomes:

$$T(E) = \frac{4\Gamma_L\Gamma_R}{(\Gamma_L+\Gamma_R)^2} \qquad (2.6.15)$$

Let $\Gamma_L >> \Gamma_R$ then we get:

$$T(E) = \frac{4\Gamma_L\Gamma_R}{(\Gamma_L)^2} \quad \rightarrow T(E) = \frac{4\Gamma_L}{{\Gamma_L}^2} << 1$$

This means that the transmission coefficient will be less than 1 if the coupling to the 'molecule' is not symmetric.

2.6.2 Fano Resonances

Molecule with a side group produce a Fano resonance when the energy *E* of the incident electron is close to an energy level when a bound state (e.g. a pendant group ε_2) is coupled (by coupling integral α) to a continuum of states as shown in figure (2.6.3). A Fano resonance is usually denoted by a resonance showing the typical Fano line shape which is a resonance followed by an anti-resonance.

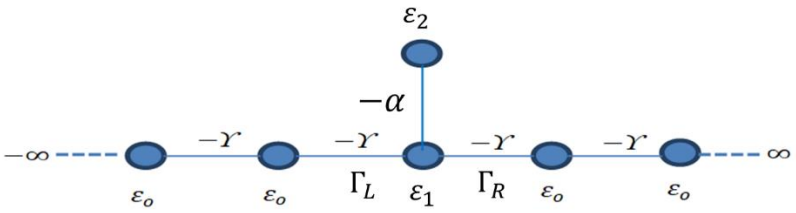

Figure 2.6.3: Simple model to study Fano resonances. Two one-dimensional semi-infinite crystalline chains coupled to a scatting region of site energy ε_1 by hopping elements Γ_L and Γ_R. An extra energy level, ε_2, is coupled to the scattering level by hopping element $-\alpha$.

By using the formula in equation (2.6.16), I calculated the transmission probabilities. The width of Fano resonances become narrow by varying the α coupling and the Fano resonances occur at $E = \varepsilon_2$.

$$T(E) = \frac{4\,\Gamma_L\,\Gamma_R}{\left(E\text{-}\varepsilon_1\text{-}\frac{\alpha\alpha^*}{E\text{-}\varepsilon_2}\right)^2 + (\Gamma_L + \Gamma_R)^2} \qquad (2.6.16)$$

2.6.3 Anti-Resonances

One of the important features in the transmission probability curve is an anti-resonance which appears when the system is multi-branched and destructive interference occurs between propagating waves at the nodal point.

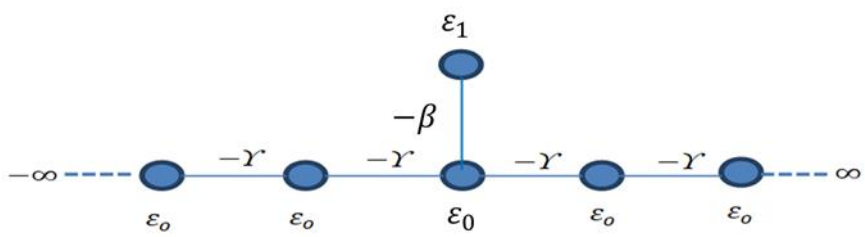

Figure 2.6.4: illustrates a simple model to study anti-resonances. One atomic site with energy ε_1 is attached to the 1-D crystalline chain with a coupling β.

Using the tight binding model to study the single electron transport properties of a one-dimensional (1-D) chain with a dangling bond.

Sending an electron through the lattice shown in figure (2.6.4) with energy $E = \varepsilon_1$ or equal to diagonal energy, then β will be infinite and *T(E)* will be equal to zero. Which means the transmission coefficient is completely destroyed when the energy level lies exactly in the site of chain. This is called destructive interference and results in an anti-resonance in the transmission spectrum. Figure (2.6.5) shows the general shape of the transmission probability related to the different kind of resonance.

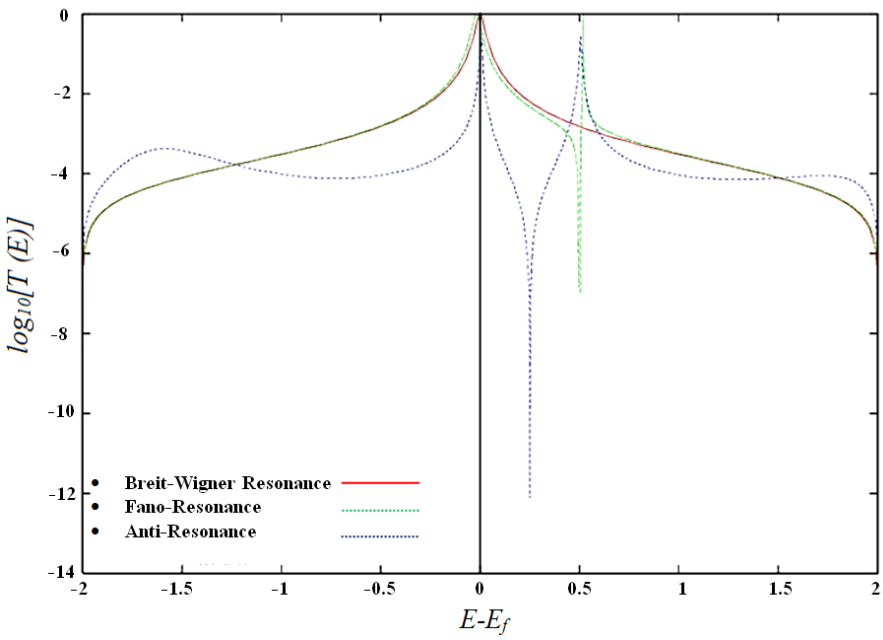

Figure 2.6.5: Transmission coefficients for the systems; Breit-Wigner (red), Fano-resonance (green) and anti-resonance (blue).

Bibliography

(1) Landauer, R. Spatial Variation of Currents and Fields Due to Localized Scatterers in Metallic Conduction. *IBM J. Res. Dev.* **1957**, *1* (3), 223–231.

(2) Büttiker, M.; Imry, Y.; Landauer, R.; Pinhas, S. Generalized Many-Channel Conductance Formula with Application to Small Rings. *Phys. Rev. B* **1985**, *31* (10), 6207.

(3) Datta, S. *Electronic Transport in Mesoscopic Systems*; Cambridge university press, 1997.

(4) Cuevas, J. C.; Scheer, E.; Cao, G.; Wang, Y.; Diagnostics, P. M. World Scientific Series in Nanoscience and Nanotechnology. **2010**.

(5) Duan, F.; Guojun, J. *Introduction To Condensed Matter Physics: Volume 1*; World Scientific Publishing Company, 2005.

(6) Lesovik, G. Electronic Transport in Meso-and Nano-Scale Conductors.

(7) Economou, E. N. *Green's Functions in Quantum Physics*; Springer, 1983; Vol. 3.

(8) Mello, P. A.; Mello, P. A.; Kumar, N.; Narendra Kumar, D. *Quantum Transport in Mesoscopic Systems: Complexity and Statistical Fluctuations, a Maximum-Entropy Viewpoint*; Oxford University Press on Demand, 2004.

(9) Sanvito, S.; Lambert, C. J.; Jefferson, J. H.; Bratkovsky, A. M. General Green's-Function Formalism for Transport Calculations with Spd Hamiltonians and Giant Magnetoresistance in Co-and Ni-Based Magnetic Multilayers. *Phys. Rev. b* **1999**, *59* (18), 11936.

(10) Breit, G.; Wigner, E. Capture of Slow Neutrons. *Phys. Rev.* **1936**, *49* (7), 519.

(11) Stadler, R. Quantum Interference Effects in Electron Transport through Nitrobenzene with Pyridil Anchor Groups. *Phys. Rev. B* **2009**, *80* (12), 125401.

(12) Ke, S.-H.; Yang, W.; Baranger, H. U. Quantum-Interference-Controlled

Molecular Electronics. *Nano Lett.* **2008**, *8* (10), 3257–3261.

(13) Papadopoulos, T. A.; Grace, I. M.; Lambert, C. J. Control of Electron Transport through Fano Resonances in Molecular Wires. *Phys. Rev. b* **2006**, *74* (19), 193306.

(14) Fano, U. Effects of Configuration Interaction on Intensities and Phase Shifts. *Phys. Rev.* **1961**, *124* (6), 1866.

(15) Petkov, V. and M. Zworski, Breit–Wigner Approximation and the Distribution of Resonances. Communications in mathematical physics, 1999. **204**(2): p. 329-351.

Chapter 3

Magic number theory and Wigner delay times in graphene-like molecules

The Wigner delay time function was proposed by Wigner in 1955 for a single scattering channel derived from a Hermitian operator based on the scattering amplitude and then generalized by Smith in 1960 to the multichannel scattering matrices. Here we study the connectivity dependence of the Wigner delay time of single-molecule junctions we study examples where the phase θ(E) of the transmission amplitude plays a crucial role in normal junctions. In this case, the phase θ(E) is related to the Wigner delay time, which characterises the time taken for an electron to pass through a single-molecule junction formed from normal electrodes. The results presented in this chapter were submitted to The Journal of Physical Chemistry.

3.1. Introduction

During the past decade, experimental and theoretical studies of single molecules attached to metallic electrodes have demonstrated that room-temperature electron transport is controlled by quantum interference (QI) within the core of the molecule[1–19]. These studies provide tremendous insight into the mechanisms leading to efficient charge transport, but they ignore key aspects of quantum mechanical phase. For example, such junctions are often described using the Landauer formula $G = G_0 T(E_F)$, where $G_0 = \frac{2e^2}{h}$ is the quantum of conductance and E_F is the Fermi energy of the electrodes. In this expression $T(E)$ is the transmission coefficient describing the probability that an electron of energy E can pass through the junction from one electrode to the other and for single-channel leads, is related to the transmission amplitude $t(E)$ by $T(E) = |t(E)|^2$, where $t(E)$ is a complex number of the form $t(E) = |t(E)|e^{i\theta(E)}$. Clearly the phase $\theta(E)$ of the transmission amplitude plays no role when computing $T(E)$, even though $T(E)$ is a result of interference from different transport channels within a molecular junction. The aim of the present study is to examine examples of molecular-scale transport in which phase plays a crucial role and to discuss aspects of molecular-scale electron transport. in normal electrode/molecule/ normal electrode N-M-N junctions. In this case, the phase $\theta(E)$ is related to the Wigner delay time, which characterises the time taken for an electron to pass through a single-molecule junction formed from normal electrodes.

3.2. Method

To illustrate how these phase-dependent phenomena can be predicted using magic number theory, figure (3.2.1) shows two examples of molecules with a graphene-like anthanthrene core, connected via triple bonds and pyridyl anchor groups to gold

electrodes. The anthanthrene core (represented by a lattice of 6 hexagons) of molecule **1** and the anthanthrene core of molecule **2** are connected differently to the triple bonds.

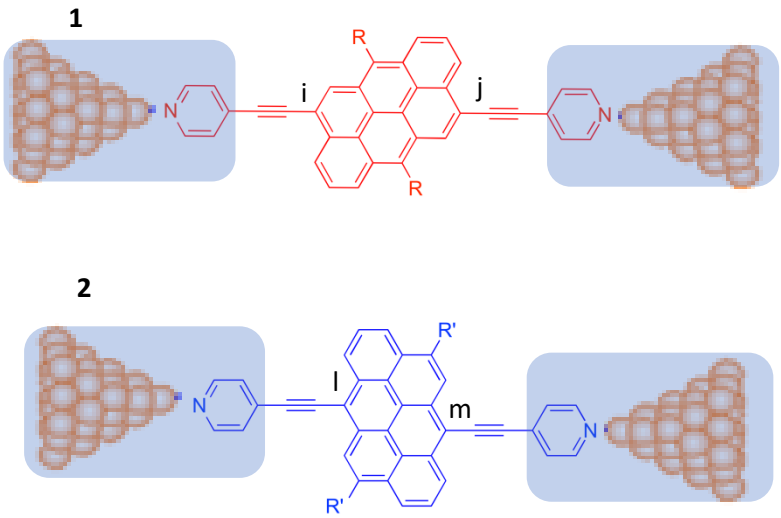

Figure (3.2.1): Examples of molecules with anthanthrene cores, connected via triple bonds and pyridyl anchor groups to the tips of gold electrodes, which in turn connect to crystalline gold leads (not shown). Molecule **1** has a connectivity *i-j* and electrical conductance σ_{ij}, while molecule **2** has a connectivity *l-m* and electrical conductance σ_{lm}.

In a typical experiment using mechanically controlled break junctions or STM break junctions[17,19], fluctuations and uncertainties in the coupling to normal-metallic electrodes are dealt with by measuring the conductance of such molecules many thousands of times and reporting the statistically-most-probable electrical conductance. If σ_{ij} is the statistically-most-probable conductance of a molecule such as 1 in figure (3.2.1), with connectivity *i-j* and σ_{lm} is the corresponding conductance of a molecule such as **2** in figure (3.2.1), with connectivity *l-m*, then it was recently predicted theoretically and demonstrated experimentally[13,20,21] that for polyaromatic hydrocarbons such as anthanthrene, the statistically-most-probable conductance ratio σ_{ij}/σ_{lm} is independent of

the coupling to the electrodes and could be obtained from tables of "magic numbers." If M_{ij} (M_{lm}) is the magic number corresponding to connectivity *i-j* (*l-m*), then this "magic ratio theory" predicts

$$\frac{\sigma_{ij}}{\sigma_{lm}} = \left(\frac{M_{ij}}{M_{lm}}\right)^2 \tag{3.2.1}$$

From a conceptual viewpoint, magic ratio theory views the shaded regions in figure (3.2.1) as "compound electrodes", comprising both the anchor groups and gold electrodes, and focuses attention on the contribution from the core alone. As discussed in Ref[22], the validity of Eq. (3.2.1) rests on the key foundational concepts of weak coupling, locality, connectivity, mid-gap transport, phase coherence and connectivity-independent statistics. When these conditions apply, the complex and often uncontrolled contributions from electrodes and electrode-molecule coupling cancel in conductance ratios and therefore a theory of conductance ratios can be developed by focusing on the contribution from molecular cores alone.

The term "weak coupling" means that the central aromatic subunit such as anthanthrene should be weakly coupled to the anchor groups *via* spacers such as acetylene, as shown in figure (3.2.1). Weak coupling means that the level broadening Γ and the self energy Σ of the HOMO and LUMO should be small compared with the HOMO-LUMO gap E_{HL}. Any corrections will then be of order Γ/E_{HL} or Σ/E_{HL}, which means that such terms can be ignored, provided the Fermi energy lies within the gap. Clearly a central condition for the applicability of the Landauer formula and therefore magic-number theory is that the molecular junction is described by a time independent mean-field Hamiltonian. The concept of 'mid-gap transport' is recognition of the fact that unless a molecular junction is externally gated by an electrochemical environment or an electrostatic gate, charge transfer between the electrodes and molecule ensures that the energy levels adjust such

that the Fermi energy E_F of the electrodes is located in the vicinity of the centre of the HOMO-LUMO gap and therefore transport takes place in the co-tunnelling regime. In other words, transport is usually 'off-resonance' and the energy of electrons passing through the core does not coincide with an energy level of the molecule. Taken together, these conditions ensure that when computing the Green's function of the core, the contribution of the electrodes can be ignored. The concept of 'phase coherence' recognises that in this co-tunnelling regime, the phase of electrons is usually preserved as they pass through a molecule and therefore transport is controlled by QI. 'Locality' means that when a current flow through an aromatic subunit, the points of entry and exit are localised in space. For example, in molecule **1** (see figure (3.2.1)), the current enters at a particular atom *i* and exits at a particular atom *j*. The concept of 'connectivity' recognises that through chemical design and synthesis, spacers can be attached to different parts of a central subunit with atomic accuracy and therefore it is of interest to examine how the flow of electricity depends on the choice of connectivity to the central subunit. The condition of "connectivity-independent statistics" means that the statistics of the coupling between the anchor groups and electrodes should be independent of the coupling to the aromatic core. To be more precise, we note that in an experimental measurement of single-molecule conductance using for example a mechanically-controlled break junction, many thousands of measurements are made and a histogram of logarithmic conductances is constructed. This statistical variation arises from variability in the electrode geometry and in the binding conformation to the electrodes of terminal atoms such as the nitrogen in figure (3.2.1). The assumption of "connectivity-independent statistics" means that this variability is the same for the two different connectivities of figure (3.2.1). When each of these conditions applies, it can be shown[13,20,21] that in the presence of normal-metallic electrodes, the most probable

electrical conductance corresponding to connectivity *i-j* is proportional to $|g_{ij}(E_F)|^2$ where $g_{ij}(E_F)$ is the Green's function of the isolated core alone, evaluated at the Fermi energy of the electrodes. In the absence of time-reversal symmetry breaking, $g_{ij}(E_F)$ is a real number. Since only conductance ratios are of interest, we define magic numbers by

$$M_{ij} = Ag_{ij}(E_F) \tag{3.2.2}$$

where *A* is an arbitrary constant of proportionality, chosen to simplify magic number tables and which cancels in Eq. (3.2.1). Magic ratio theory represents an important step forward, because apart from the Fermi energy E_F, no information about the electrodes is required. The question we address below is how can the theory be extended to describe Wigner delay times?

In the presence of normal-metallic electrodes, many papers discuss the conditions for *destructive* quantum interference (DQI), for which $M_{ij} \approx 0$ [5,7,17,23–27]. On the other hand, magic ratio theory aims to describe *constructive* quantum interference (CQI), for which M_{ij} may take a variety of non-zero values. If H is the non-interacting Hamiltonian of the core, then since $g(E_F) = (E_F\text{-}H)^{-1}$, the magic number table is obtained from a matrix inversion, whose size and complexity reflects the level of detail contained in H. The quantities M_{ij} were termed "magic" [13,20,21], because even a simple theory based on connectivity alone yields values, which are in remarkable agreement with experiment[20] . For example, for molecule **1** (see figure (3.2.1)), the prediction was $M_{ij} = -1$, whereas for molecule **2**, $M_{lm} = -9$ and therefore the electrical conductance of molecule **2** was predicted to be 81 times higher than that of **1**, which is close to the measured value of 79. This large ratio is a clear manifestation of quantum interference (QI), since such a change in connectivity to a classical resistive network would yield only a small change in

conductance. To obtain the above values for M_{ij} and M_{lm}, the Hamiltonian H was chosen to be

$$H = \begin{pmatrix} 0 & C \\ C^t & 0 \end{pmatrix} \tag{3.2.3}$$

where the connectivity matrix C of anthanthrene is shown in figure (3.2.2). In other words, each element H_{ij} was chosen to be -1 if i, j are nearest neighbours or zero otherwise and since anthanthrene is represented by the bipartite lattice in which odd numbered sites are connected to even numbered sites only, H is block off-diagonal. The corresponding core Green's function evaluated at the gap centre $E_F = 0$ is therefore obtained from a simple matrix inversion $g(0) = -H^{-1}$. Since H and therefore $-H^{-1}$ are block off-diagonal, this yields $M = \begin{pmatrix} 0 & \bar{M}^t \\ \bar{M} & 0 \end{pmatrix}$, where M is the magic number table of the polycyclic aromatic hydrocarbons (PAHs) core. The connectivity matrix C and off-diagonal block of the magic number table $\bar{M}$ for anthanthrene are shown in Figure *(***3.2.2**b and c respectively. As noted above, for molecule **1**, with connectivity 9-22, $M_{9,22} = -1$, whereas for molecule **2**, with connectivity 3-12, $M_{3,12} = -9$.

a

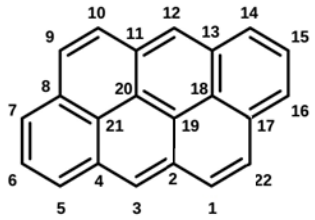

b

C	2	4	6	8	10	12	14	16	18	20	22
1	-1	0	0	0	0	0	0	0	0	0	-1
3	-1	-1	0	0	0	0	0	0	0	0	0
5	0	-1	-1	0	0	0	0	0	0	0	0
7	0	0	-1	-1	0	0	0	0	0	0	0
9	0	0	0	-1	-1	0	0	0	0	0	0
11	0	0	0	0	-1	-1	0	0	0	-1	0
13	0	0	0	0	0	-1	-1	0	-1	0	0
15	0	0	0	0	0	0	-1	-1	0	0	0
17	0	0	0	0	0	0	0	-1	-1	0	-1
19	-1	0	0	0	0	0	0	0	-1	-1	0
21	0	-1	0	-1	0	0	0	0	0	-1	0

c

M	1	3	5	7	9	11	13	15	17	19	21
2	-1	-7	4	-4	1	-1	1	-1	1	-2	3
4	1	-3	-4	4	-1	1	-1	1	-1	2	-3
6	-1	3	-6	-4	1	-1	1	-1	1	-2	3
8	1	-3	6	-6	-1	1	-1	1	-1	2	-3
10	-1	3	-6	6	-9	-1	1	-1	1	-2	3
12	3	-9	8	-8	7	-7	-3	3	-3	6	1
14	-6	8	-6	6	-4	4	-4	-6	6	-2	-2
16	6	-8	6	-6	4	-4	4	-4	-6	2	2
18	3	1	-2	2	-3	3	-3	3	-3	-4	1
20	-2	6	-2	2	2	-2	2	-2	2	-4	-4
22	-9	7	-4	4	-1	1	-1	1	-1	2	-3

Figure (3.2.2): (a) The anthanthrene cores numbering system. (b) The connectivity table C. (c) The non-interacting magic number table $\overline{M}$ corresponding to the anthanthrene lattice.

Magic number tables such as Figure (3.2.2c) are extremely useful, since they facilitate the identification of molecules with desirable conductances for future synthesis. Conceptually, tables obtained from Hamiltonians are also of interest, since they capture the contribution from intra-core connectivity alone (via the matrix C, comprising -1's or zeros), while avoiding the complexities of chemistry.

3.3. Results and discussion

The Wigner delay time function was proposed by Wigner in 1955 for a single scattering channel derived from a Hermitian operator based on the scattering amplitude and then generalized by Smith in 1960 to the multichannel scattering matrices[28–30].

Consider a scatterer whose transmission amplitude is $t_{ab}(E) = |t_{ab}(E)| \times e^{i\theta_{ab}(E)}$. The corresponding Wigner delay time τ_W is define by $\tau_W = \hbar\tau_{ab}$, where

$$\tau_{ab} = \frac{d\theta_{ab}}{dE} \tag{3.3.1}$$

If the scatterer is connected to single-channel current-carrying electrodes by couplings γ_a and γ_b, it can be show that

$$t_{ab}(E) = 2i \sin k \times e^{2ik} \times \left(\frac{\gamma_a \times \gamma_b}{\gamma}\right) \times \frac{g_{ab}}{\Delta} \tag{3.3.2}$$

Where

$$\Delta = 1 + \frac{\gamma_a^2}{\gamma} g_{aa}\, e^{ik} + \frac{\gamma_b^2}{\gamma} g_{bb}\, e^{ik} + \frac{\gamma_a^2 \gamma_b^2}{\gamma^2} (g_{aa}\, g_{bb} - g_{ab} g_{ba})\, e^{2ik} \tag{3.3.3}$$

In deriving this expression, the electrodes are assumed to be one-dimensional tight-binding chains, with nearest neighbour hopping elements $-\gamma$, (where $\gamma > 0$) with a dispersion relation $E = -2\gamma \cos k$, which relates the energy E of an electron travelling along the electrode to its wave vector k, where $0 \leq k \leq \pi$. The group velocity of such electrons within the electrodes is therefore $v = \frac{dE}{dk} = 2\gamma \sin k$.

In equation (3.3.3), γ_a, γ_b are the couplings between molecule and the left and right electrodes respectively. g_{ab} is the a, b element of the core Green's function $g = (E-H)^{-1}$, where *H* is the Hamiltonian describing the isolated core. Since we are interested in the contribution to the delay time from the molecular core, we shall consider the 'wide band limit', where k is independent of energy E in the energy range of interest, between the highest occupied molecular orbital (HOMO) and lowest unoccupied molecular orbital (LUMO) of the scattering region formed by the molecule. When *H* is real g is real and

therefore the delay time is obtained from the phase of the complex number $\Delta = 1 + \Delta_1 + i\Delta_2$.

In this expression, $\Delta_1 = \alpha \cos k + \beta \cos 2k$, $\Delta_2 = \alpha \sin k + \beta \sin 2k$ where, $\alpha = \frac{\gamma_a{}^2}{\gamma} g_{aa} + \frac{\gamma_b{}^2}{\gamma} g_{bb}$ and $\beta = \frac{\gamma_a{}^2 \gamma_b{}^2}{\gamma^2} (g_{aa}\, g_{bb} - g_{ab}\, g_{ba})$. Hence $\theta_{ab} = -\mathrm{atan}(\frac{\Delta_2}{1+\Delta_1})$ and

$$\tau_{ab} = -\left[\frac{\dot{\Delta}_2(1+\Delta_1) - \dot{\Delta}_1\Delta_2}{(1+\Delta_1)^2 + \Delta_2^2}\right]$$

$$= -\left[\frac{\dot{\alpha}\sin k + \dot{\beta}\sin 2k + (\dot{\beta}\alpha - \dot{\alpha}\beta)\sin k}{(1+\alpha\cos k + \beta\cos 2k)^2 + (\alpha\sin k + \beta\sin 2k)^2}\right] \qquad (3.3.4)$$

As an example, consider the mathematically simple ballistic limit, where the scatterer is a linear chain of *N* sites coupled by nearest neighbor elements $-\gamma$. In this case, by choosing $\gamma_a = \gamma_b = \gamma$, the system reduces to a perfect linear crystal and one obtains $\theta_{ab} = k(N+1) + \frac{\pi}{2}$ and $\tau_{ab} = \frac{(N+1)dk}{dE} = \frac{N+1}{v}$, where $v = \frac{dE}{dk} = 2\gamma \sin k$ is the group velocity of a wave packet of energy E. In other words, one obtains the intuitive result that the delay time is the length of the scatterer divided by the group velocity.

On the other hand, we are interested in the opposite limit of a scatterer, which is weakly coupled to the leads, such that $\frac{\gamma_a}{\gamma} \ll 1$ and $\frac{\gamma_b}{\gamma} \ll 1$ and transport is off-resonance, such that the energy E lies within the HOMO-LUMO gap. In this case, $\beta \ll \alpha$, and $\alpha \ll 1$ so the delay time reduces to

$$\tau_{ab} \approx -\dot{\alpha}\sin k \approx -\left(\dot{g}_{bb}\frac{\gamma_b{}^2}{\gamma} + \dot{g}_{aa}\frac{\gamma_a{}^2}{\gamma}\right)\sin k \qquad (3.3.5)$$

This equation shows that the total delay time is a sum of independent times due to each contact.

$$\tau_{ab} \approx (\tau_{bb}\frac{\gamma_b{}^2}{\gamma} + \tau_{aa}\frac{\gamma_a{}^2}{\gamma})\sin k \qquad (3.3.6)$$

where we have defined an intrinsic core delay time to be:

$$\tau_{aa} = -\dot{g}_{aa} \tag{3.3.7}$$

which is independent of the coupling to the leads. Since $g_{aa} = \sum_{n=1}^{N} \frac{[\psi_a(n)]^2}{E-\lambda_n}$,

this yield

$$\tau_{aa} = (g^2)_{aa} = \sum_{n=1}^{N} \frac{[\psi_a(n)]^2}{(E-\lambda_n)^2} \tag{3.3.8}$$

Since the local density of states ρ_a is given by $\rho_a = -1/\pi \mathrm{Lt}_{\eta\to 0}\, \mathrm{Im} \sum_{n=1}^{N} \frac{\psi_a(n)\psi_b(n)}{E-\lambda_n+i\eta} = \eta/\pi \sum_{n=1}^{N} \frac{[\psi_a(n)]^2}{(E-\lambda_n)^2+\eta^2}$, this demonstrates that τ_{aa} is proportional to the local density of states at atom a of the isolated molecule.

In the case where the couplings to the leads (γ_a and γ_b) are identical, then the ratio of delay times corresponding to connectivities a, b and c, d is

$$\frac{\tau_{ab}}{\tau_{cd}} = \frac{\tau_{aa} + \tau_{bb}}{\tau_{cc} + \tau_{dd}} \tag{3.3.9}$$

This delay time ratio is a property of the core Green's function g alone. It is interesting to note that as illustrated by all the above examples, in the weak coupling limit, the delay time is always positive.

Since $\tau_{aa} = -\dot{g}_{aa}$, where $g = (E-H)^{-1}$, τ_{aa} is obtained from the diagonal elements of $-\dot{g} = (E-H)^{-2}$, which at $E = 0$ is proportional to M^2, where M is the core of the magic number table.

3.4. Calculation of the Wigner delay times for on-resonance transport

In the absence of external gating, electron transport through molecules under ambient conditions is usually off-resonance. On the other hand, if a molecule is gated such that the energy E of electrons passing through the molecule is close to an energy level of the molecule, then in principle transport could be on resonance. To illustrate the properties of τ_{ab} in this limit, we now examine a number of examples, under the condition that the scatterer is weakly coupled to the leads, such that $\frac{\gamma_a}{\gamma} \ll 1$ and $\frac{\gamma_b}{\gamma} \ll 1$.

<u>Example 1a:</u>

In the limit $\beta \ll \alpha$, equation (3.3.4) reduces to

$$\tau_{ab} \approx -\left[\frac{\dot{\alpha}\sin k}{(1+\alpha\cos k)^2+(\alpha\sin k)^2}\right] \tag{3.3.10}$$

As an example, consider the case where

$$g_{ab} \approx \frac{\psi_a\psi_b}{E-\lambda_0} \tag{3.3.11}$$

In this case, $\beta = 0$ and

$$\tau_{ab} \approx \left[\frac{\Gamma_{ab}}{(E-\lambda_{ab})^2+\Gamma_{ab}^2}\right] \tag{3.3.12}$$

In this expression, $\lambda_{ab} = \lambda_0 - \sigma$, $\sigma = \sigma_a + \sigma_b$ and $\Gamma_{ab} = \Gamma_a + \Gamma_b$, where $\sigma_a = -\frac{\gamma_a{}^2}{\gamma}\psi_a^2\cos k$ and $\Gamma_a = \frac{\gamma_a{}^2}{\gamma}\psi_a^2\sin k$ and similarly for σ_b, Γ_b. Hence on resonance, where $E = \lambda_{ab}$, the delay time reduces to $\tau_{ab} \approx 1/\Gamma_{ab}$. On the other hand, if transport is off resonance and E lies close to the gap centre,

$\tau_{ab} \approx \frac{\Gamma_{ab}}{\delta^2}$, where $\delta$is half the HOMO-LUMO gap. Since $\Gamma_{ab} \ll \delta$, this demonstrates that the 'on-resonance' delay time is much longer than the 'off-resonance' delay time.

Interestingly, the transmission coefficient $T_{ab}(E) = |t_{ab}|^2$ in this case is given by the Breit-Wigner formula:

$$T_{ab} \approx \left[\frac{4\Gamma_a\Gamma_b}{(E\text{-}\lambda_{ab})^2 + \Gamma_{ab}^2}\right] \tag{3.3.13}$$

Hence the delay time is related to the electrical conductance by

$$T_{ab}/\tau_{ab} \approx \frac{4\Gamma_a\Gamma_b}{\Gamma_a + \Gamma_b} \tag{3.3.14}$$

Example 1b:

As a further example, consider the case of a Fano resonance created by a pendant orbital of energy ϵ coupled to ψ by a coupling constant η, such that $\lambda_0 = \lambda_1 + \eta^2/(E\text{-}\epsilon)$. In this case, since λ_0 is energy dependent, one obtains

$$\tau_{ab} \approx \frac{\Gamma_{ab}\left(1 + \frac{\eta^2}{(E\text{-}\epsilon)^2}\right)}{\left(E\text{-}\lambda_{ab}\text{-}\frac{\eta^2}{(E\text{-}\epsilon)^2}\right)^2 + \Gamma_{ab}^2} \tag{3.3.15}$$

Near the Fano resonance, where $E \approx \epsilon$, this yields

$$\tau_{ab} \approx \frac{\Gamma_{ab}}{\eta^2} \tag{3.3.16}$$

For $\eta \ll \Gamma_{ab}$, this yields $\tau_{ab} \gg 1/\Gamma_{ab}$, which means that the electron spends a long time on the pendant orbital.

In this case,

$$T_{ab}/\tau_{ab} \approx \frac{4\Gamma_a\Gamma_b}{(\Gamma_a + \Gamma_b)\left(1 + \frac{\eta^2}{(E\text{-}\epsilon)^2}\right)} \tag{3.3.17}$$

Which reflects the fact that T_{ab} vanishes at the Fano resonance, where $E = \epsilon$.

As examples, consider the graphene-like molecules shown in Figure (3.4.1), in which (a) represents a benzene ring, (b) naphthalene, (c) anthracene, (d) tetracene, (e) pentacene (f) pyrene, (g) anthanthrene and (k) azulene.

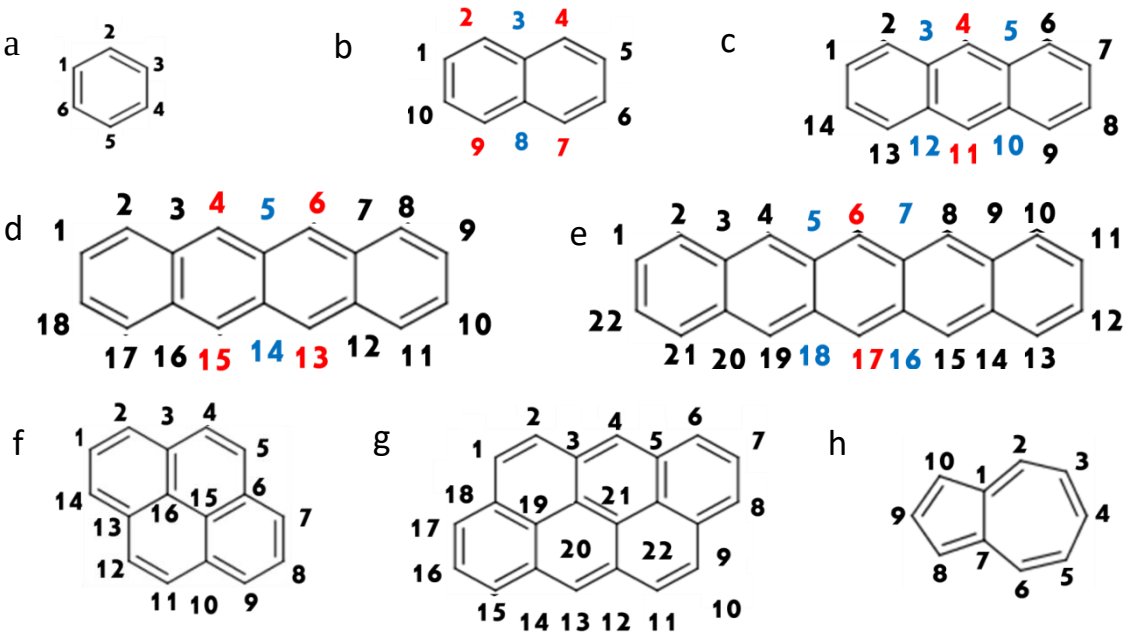

Figure (3.4.1): Molecular structure of substituted: a) benzene ring, b) a naphthalene, c) anthracene, d) tetracene, e) pentacene, f) pyrene, g) anthanthrene and h) azulene.

For the naphthalene core shown in Figure (3.4.2,a), the τ_{ij} table of Figure (3.4.2b), describes Wigner delay times in the middle of HOMO-LUMO gap.

a

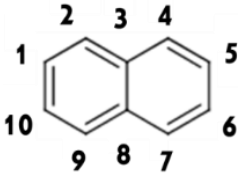

b

τij	1	2	3	4	5	6	7	8	9	10
1	-0.89	0.00	0.22	0.00	0.11	0.00	-0.44	0.00	0.56	0.00
2	0.00	-1.22	0.00	0.78	0.00	-0.44	0.00	0.11	0.00	0.56
3	0.22	0.00	-0.56	0.00	0.22	0.00	0.11	0.00	0.11	0.00
4	0.00	0.78	0.00	-1.22	0.00	0.56	0.00	0.11	0.00	-0.44
5	0.11	0.00	0.22	0.00	-0.89	0.00	0.56	0.00	-0.44	0.00
6	0.00	-0.44	0.00	0.56	0.00	-0.89	0.00	0.22	0.00	0.11
7	-0.44	0.00	0.11	0.00	0.56	0.00	-1.22	0.00	0.78	0.00
8	0.00	0.11	0.00	0.11	0.00	0.22	0.00	-0.56	0.00	0.22
9	0.56	0.00	0.11	0.00	-0.44	0.00	0.78	0.00	-1.22	0.00
10	0.00	0.56	0.00	-0.44	0.00	0.11	0.00	0.22	0.00	-0.89

Figure (3.4.2): a) Molecule structure of naphthalene with numbering. b) The τ_{ab} table of naphthalene. Note that by symmetry, there are only three distinct delay times.

To demonstrate how the Wigner delay times change with the number of the rings in the acene series a-e of Figure (3.4.1), we calculate the maximum and minimum delay times for each core as a function of the number of rings. For structures shown in Figure (3.4.1)a-e), shows the maximum and minimum of the Wigner delay times, corresponding to the connectivities marked red and blue respectively. For example, in Figure (3.4.1)b), for naphthalene, the maximum delay time is corresponding to atoms number 2, 4, 9, 7 and atoms 3 and 8 have the minimum value.

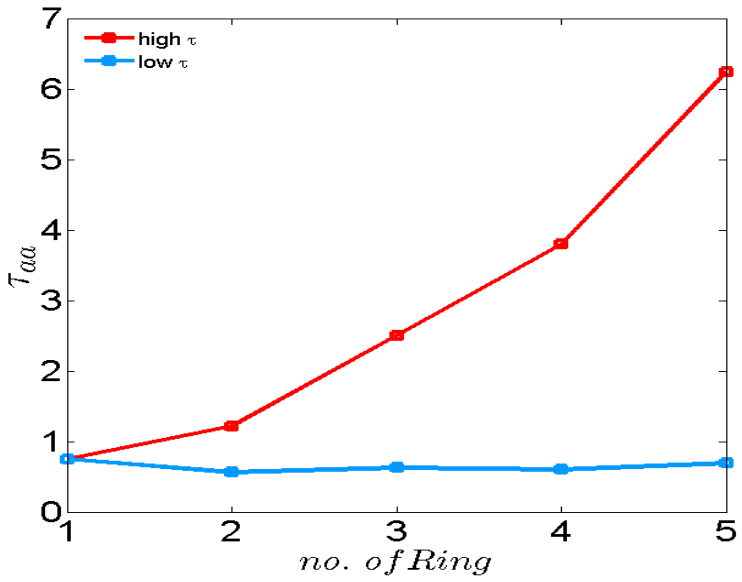

Figure (3.4.3): The maximum and minimum values of τ_{aa} for the acene series as a function of the number of rings.

The following table summarize the min-max value of τ for different molecules.

Molecular heart	max of τ_{aa}	min of τ_{aa}
Benzene	0.75	0.75
Naphthalene	1.22	0.55
Anthracene	2.5	0.62
4_rings	3.8	0.8
5_rings	6.25	0.69
Pyrene	1.75	0.67
Anthanthrene	3.8	0.6
Azulene	1.97	1.18

Table (3.4.1): Maximum and minimum core delay times for the molecules of figure (3.4.1).

The above behavior is clearly reflected in the local density of states of the molecules, shown in figure (3.4.4).

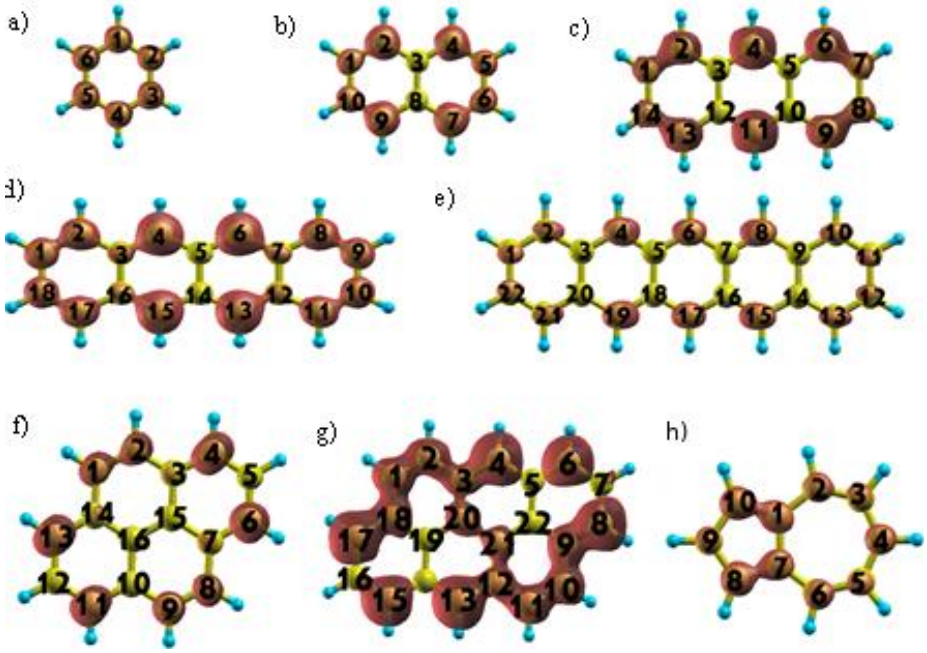

Figure (3.4.4): The local density of states of the molecules shown in Figure (3.4.1).

Bibliography

(1) Sadeghi, H.; Mol, J. a; Lau, C. S.; Briggs, G. A. D.; Warner, J.; Lambert, C. J. Conductance Enlargement in Picoscale Electroburnt Graphene Nanojunctions. *Proc. Natl. Acad. Sci. USA* **2015**, *112* (9), 2658–2663.

(2) Manrique, D. Z.; Huang, C.; Baghernejad, M.; Zhao, X.; Al-Owaedi, O. A.; Sadeghi, H.; Kaliginedi, V.; Hong, W.; Gulcur, M.; Wandlowski, T.; et al. A Quantum Circuit Rule for Interference Effects in Single-Molecule Electrical Junctions. *Nat. Commun.* **2015**, *6*, 6389.

(3) Solomon, G. C.; Bergfield, J. P.; Stafford, C. A.; Ratner, M. A. When small Terms Matter: Coupled Interference Features in the Transport Properties of Cross-Conjugated Molecules. *Beilstein J. Nanotechnol.* **2011**, *2*, 862.

(4) Sedghi, G.; García-Suárez, V. M.; Esdaile, L. J.; Anderson, H. L.; Lambert, C. J.; Martín, S.; Bethell, D.; Higgins, S. J.; Elliott, M.; Bennett, N.; et al. Long-Range Electron Tunnelling in Oligo-Porphyrin Molecular Wires. *Nat. Nanotechnol.* **2011**, *6* (8), 517–523.

(5) Ricks, A. B.; Solomon, G. C.; Colvin, M. T.; Scott, A. M.; Chen, K.; Ratner, M. A.; Wasielewski, M. R. Controlling Electron Transfer in Donor- Bridge- Acceptor Molecules Using Cross-Conjugated Bridges. *J. Am. Chem. Soc.* **2010**, *132* (43), 15427–15434.

(6) Magoga, M.; Joachim, C. Conductance of Molecular Wires Connected or Bonded in Parallel. *Phys. Rev. B* **1999**, *59* (24), 16011.

(7) Zhao, X.; Geskin, V.; Stadler, R. Destructive Quantum Interference in Electron Transport: A Reconciliation of the Molecular Orbital and the Atomic Orbital

Perspective. *J. Chem. Phys.* **2017**, *146* (9), 92308.

(8) Sangtarash, S. Theory of Mid-Gap Quantum Transport through Single Molecule: New Approach to Transport Modeling of Nanoelectronic Devices, Lancaster University, 2017.

(9) Sadeghi, H. Theory of Electron, Phonon and Spin Transport in Nanoscale Quantum Devices. *Nanotechnology* **2018**.

(10) Bai, J.; Daaoub, A.; Sangtarash, S.; Li, X.; Tang, Y.; Zou, Q.; Sadeghi, H.; Liu, S.; Huang, X.; Tan, Z.; et al. Anti-Resonance Features of Destructive Quantum Interference in Single-Molecule Thiophene Junctions Achieved by Electrochemical Gating. *Nat. Mater.* **2019**, 1.

(11) Sangtarash, S.; Sadeghi, H.; Lambert, C. J. Exploring Quantum Interference in Heteroatom-Substituted Graphene-like Molecules. *Nanoscale* **2016**, *8* (27), 13199–13205.

(12) Lambert, C. J. Basic Concepts of Quantum Interference and Electron Transport in Single-Molecule Electronics. *Chem. Soc. Rev.* **2015**, *44* (4), 875–888.

(13) Geng, Y.; Sangtarash, S.; Huang, C.; Sadeghi, H.; Fu, Y.; Hong, W.; Wandlowski, T.; Decurtins, S.; Lambert, C. J.; Liu, S.-X. Magic Ratios for Connectivity-Driven Electrical Conductance of Graphene-like Molecules. *J. Am. Chem. Soc.* **2015**, *137* (13), 4469–4476.

(14) Arroyo, C. R.; Tarkuc, S.; Frisenda, R.; Seldenthuis, J. S.; Woerde, C. H. M.; Eelkema, R.; Grozema, F. C.; van der Zant, H. S. J. Signatures of Quantum Interference Effects on Charge Transport through a Single Benzene Ring. *Angew. Chemie* **2013**, *125* (11), 3234–3237.

(15) Zhao, X.; Huang, C.; Batsanov, A. S.; Baghernejad, M.; Hong, W.; Bryce, M. R.; Wandlowski, T. Oligo(Aryleneethynylene)s with Terminal Pyridyl Groups: Synthesis and Length Dependence of the Tunneling-to-Hopping Transition of Single-Molecule Conductances. *Chem. Mater.* **2013**, *25* (21), 4340–4347..

(16) Aradhya, S. V; Venkataraman, L. Single-Molecule Junctions beyond Electronic Transport. *Nat. Nanotechnol.* **2013**, *8* (6), 399.

(17) Guédon, C. M.; Valkenier, H.; Markussen, T.; Thygesen, K. S.; Hummelen, J. C.; Van Der Molen, S. J. Observation of Quantum Interference in Molecular Charge Transport. *Nat. Nanotechnol.* **2012**, *7* (5), 305.

(18) Aradhya, S. V; Meisner, J. S.; Krikorian, M.; Ahn, S.; Parameswaran, R.; Steigerwald, M. L.; Nuckolls, C.; Venkataraman, L. Dissecting Contact Mechanics from Quantum Interference in Single-Molecule Junctions of Stilbene Derivatives. *Nano Lett.* **2012**, *12* (3), 1643–1647.

(19) Ballmann, S.; Härtle, R.; Coto, P. B.; Elbing, M.; Mayor, M.; Bryce, M. R.; Thoss, M.; Weber, H. B. Experimental Evidence for Quantum Interference and Vibrationally Induced Decoherence in Single-Molecule Junctions. *Phys. Rev. Lett.* **2012**, *109* (5), 56801.

(20) Sangtarash, S.; Huang, C.; Sadeghi, H.; Sorohhov, G.; Hauser, J.; Wandlowski, T.; Hong, W.; Decurtins, S.; Liu, S.-X.; Lambert, C. J. Searching the Hearts of Graphene-like Molecules for Simplicity, Sensitivity, and Logic. *J. Am. Chem. Soc.* **2015**, *137* (35), 11425–11431.

(21) Sangtarash, S.; Sadeghi, H.; Lambert, C. J. Exploring Quantum Interference in Heteroatom-Substituted Graphene-like Molecules. *Nanoscale* **2016**, *8* (27), 13199–13205.

(22) Lambert, C. J.; Liu, S.-X. A Magic Ratio Rule for Beginners: A Chemist's Guide to Quantum Interference in Molecules. *Chem. Eur. J.* **2018**, *24* (17), 4193–4201.

(23) Nozaki, D.; Lucke, A.; Schmidt, W. G. Molecular Orbital Rule for Quantum Interference in Weakly Coupled Dimers: Low-Energy Giant Conductivity Switching Induced by Orbital Level Crossing. *J. Phys. Chem. Lett.* **2017**, *8* (4), 727–732.

(24) Nozaki, D.; Toher, C. Is the Antiresonance in Meta-Contacted Benzene Due to the Destructive Superposition of Waves Traveling Two Different Routes around the Benzene Ring? *J. Phys. Chem. C* **2017**, *121* (21), 11739–11746.

(25) Reuter, M. G.; Hansen, T. Communication: Finding Destructive Interference Features in Molecular Transport Junctions. AIP 2014.

(26) Garner, M. H.; Solomon, G. C.; Strange, M. Tuning Conductance in Aromatic Molecules: Constructive and Counteractive Substituent Effects. *J. Phys. Chem. C* **2016**, *120* (17), 9097–9103.

(27) Borges, A.; Fung, E.-D.; Ng, F.; Venkataraman, L.; Solomon, G. C. Probing the Conductance of the System of Bipyridine Using Destructive Interference. *J. Phys. Chem. Lett.* **2016**, *7* (23), 4825–4829.

(28) Texier, C. Wigner Time Delay and Related Concepts: Application to Transport in Coherent Conductors. *Phys. E Low-dimensional Syst. Nanostructures* **2016**, *82*, 16–33.

(29) Wigner, E. P. Lower Limit for the Energy Derivative of the Scattering Phase Shift. *Phys. Rev.* **1955**, *98* (1), 145.

(30) Smith, F. T. Lifetime Matrix in Collision Theory. *Phys. Rev.* **1960**, *118* (1), 349.

Chapter 4

Bias-driven conductance *increase* with length in porphyrin tapes

The search for long-range charge transport across individual molecules has been subject to many studies in the last couple of decades related to many chemical and physical processes. In contrast, there are no systematic experimental or theoretical studies of the effects of applied bias voltage on the length dependence of their conductance. In this chapter It is great of interest to study and investegat how the change in conductance with length of oligo(porphyrin)s with well-defined anchor groups depends on voltage. This work was carried out in collaboration with experimental groups in Oxford and Liverpool university. The results presented in this chapter were published in 'Bias-driven conductance increase with length in porphyrin tapes' J. Am. Chem. Soc. 2018, 140, 12877−12883.

4.1. Introduction

Investigating length dependence and long-range charge transport across individual molecules is an important area of study related to many chemical and physical processes. One example is in photosynthesis, where the harvesting of sunlight is achieved via stepwise electron transfer.[1] Another is the study of electron transport through protein-based junctions, which is found to be surprisingly efficient, and where the exact transport mechanism remains unclear.[2,3] Single molecule-based devices offer benefits such as switchability,[4–8] reduced power requirements and small footprints, and have the potential to transform areas such as chemical sensing, molecular logic and thermoelectric devices.[9–11] Porphyrins, which are an important part of the photosynthetic process,[1] are promising candidates for sub-10 nm electronics due to their long-range charge transport ability.[12–22] They are planar, aromatic macrocycles, and when joined together in the form of oligomers, the degree of overall conjugation, and hence HOMO-LUMO (H-L) gap, depends on the type of inter-ring connection. Connection at the *meso* positions with alkynes results in moderate electronic communication between rings.[23–25] Linking with multiple covalent bonds, on the other hand, produces much stronger effects.[18] Triply-linked (edge-fused) porphyrin tapes show remarkable electronic properties, and dramatic reductions in H-L gap with length, with some of the smallest gaps reported for organic compounds.[26] This makes them extremely interesting to study both from a fundamental point of view, to test our models of electron transfer, and more pragmatically, to test their ability as molecular wires. To the best of our knowledge, however, there have been only a couple of experimental studies into the conductance of fused porphyrins with well-defined anchor groups[13,27] and only one theoretical study.[28] Furthermore, there are no systematic experimental or theoretical studies of the effects of applied bias voltage on the length dependence of their conductance. Systematic studies into distance dependence

as a function of voltage are themselves rare, with just a few examples in the literature, mostly without well-defined anchor groups.[29–31] It is therefore of great interest to study how the change in conductance with length of oligo(porphyrin)s with well-defined anchor groups depends on voltage.

In general, for coherent transport, molecular conductance is expected to decrease exponentially with length, following the form,

$$G(l) = A \exp(-\beta l) \tag{4.1.1}$$

where l represents the molecular length, A is a pre-factor that sets the order of magnitude and β is the conductance attenuation factor which describes the degree to which the conductance decays as the length of the wire is increased.[21] For single molecules wired between a pair of metallic (normally gold) electrodes, alkanes display high β values, between 8-10 nm^{-1},[32,33] whilst oligo(phenyl)s and oligo(phenylene ethynylene)s are much lower, between 3-4 nm^{-1},[34,35] This trend clearly demonstrates that conjugation through π-bonding produces lower β values than σ-bonding, highlighting the importance of chemical structure on conductance attenuation. As conductance, however, is expected to change with voltage, it is natural to ask how the attenuation varies as a consequence. Recent theoretical analysis of zero-bias transport through fused porphyrin wires,[28] predicts that the zero bias β is sensitive to the anchor group, and for fused porphyrins connected to graphene electrodes the zero bias conductance can *increase* with increasing length. This 'negative β' is due to the quantum nature of electron transport through such wires, arising from the strong narrowing of the HOMO-LUMO gap as the length of the oligomers increases. Since the transmission coefficient depends strongly on the energy of injected electrons, a significant voltage dependence of β is anticipated.

4.2. Molecular structure

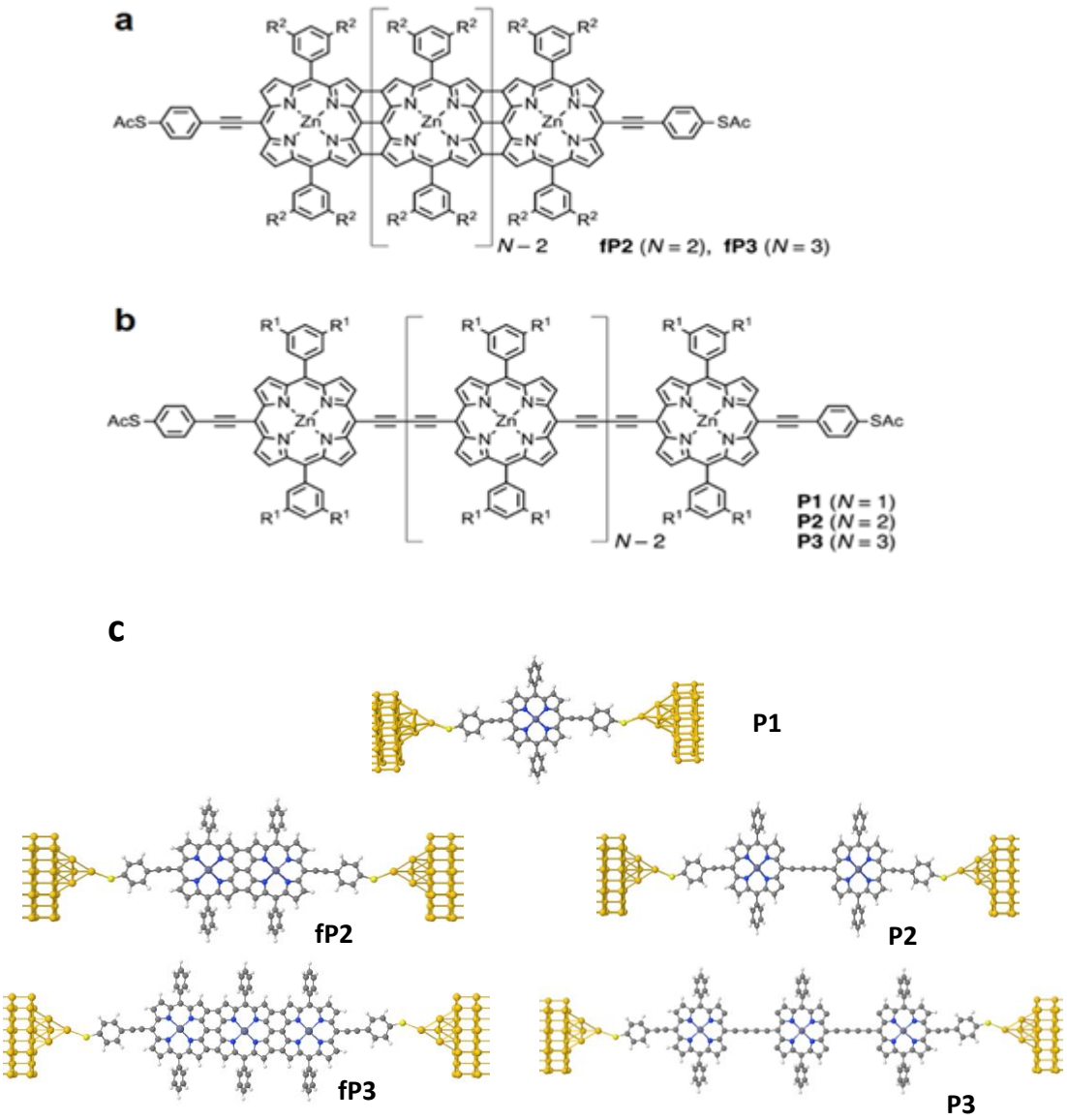

Figure 4.2.1: (a) Structure of fused porphyrins **fP2** and **fP3 (**R^2 = $Si(C_6H_{13})_3$), (b) butadiyne-linked porphyrins **P1**, **P2** and **P3 (**R^1 = OC_8H_{17}) and (c) Geometry of molecule **P1, P2, P3, fP2 and fP3** contacted between gold electrodes.

We have examined two families of porphyrin oligomers, one with moderate inter-porphyrin coupling, and the other with strong coupling. Moderate coupling is achieved via butadiyne (C4) linkers (**P1-P3** as shown in Figure (4.2.1, b)), and much stronger coupling is achieved by directly fusing the porphyrins, creating the structures shown in Figure (4.2.1, a) (**fP2** and **fP3**). The HOMO-LUMO gap decreases with length in both series, with the largest reduction seen for the fused series. The electrochemical HOMO-LUMO gaps for **fP2** and **fP3** were measured as 1.08 eV and 0.78 eV respectively.

To theoretically model the conductance of the series of porphyrin molecules attached to gold electrodes we use a first principles quantum transport approach, combining the density functional code SIESTA[36] and GOLLUM.[37] Firstly, the optimum geometry of the isolated molecule was calculated using a double-zeta polarized basis set, an energy cutoff of 150 Rydbergs, norm conserving pseudopotentials and the GGA[38] functional to describe the exchange correlation functional. The molecule was relaxed until all forces on the atoms were less than 0.1 V/Å. Gold electrodes were then attached to the molecule,

The optimum binding location was found by relaxing the molecule in the presence of the gold leads and the gold-sulphur bond distance was found to be 2.6 Å and the Au-S-C bond angle 140°. The zero bias transmission coefficient T(E) was calculated by extracting a Hamiltonian describing this molecular junction Figure (4.2.1, c) from SIESTA and utilizing the Greens function based method of GOLLUM. The conductance was then calculated from G = I/V where $I = \int_{E_F - \frac{eV}{2}}^{E_F + \frac{eV}{2}} T(E)\, dE$.

4.3. Results and discussion

Figure (4.3.1) a and b show 1D histograms at selected voltages (0.1 V and 0.7 V). experimental result carried out by our collaborators at Liverpool university . At or below 0.1 V, **P1** has the highest conductance, with **fP2** and **fP3** both being very similar. At 0.7 V, it is clear, however, that the conductance trend now becomes $G_{fP3} > G_{fP2} > G_{P1}$ due to the dependence of G on V increasing in the order **P1** < **fP2** < **fP3**. The conductance of **fP3** is not only 2.5 orders of magnitude larger than **P3**, but around a factor 20 larger than **P1**.

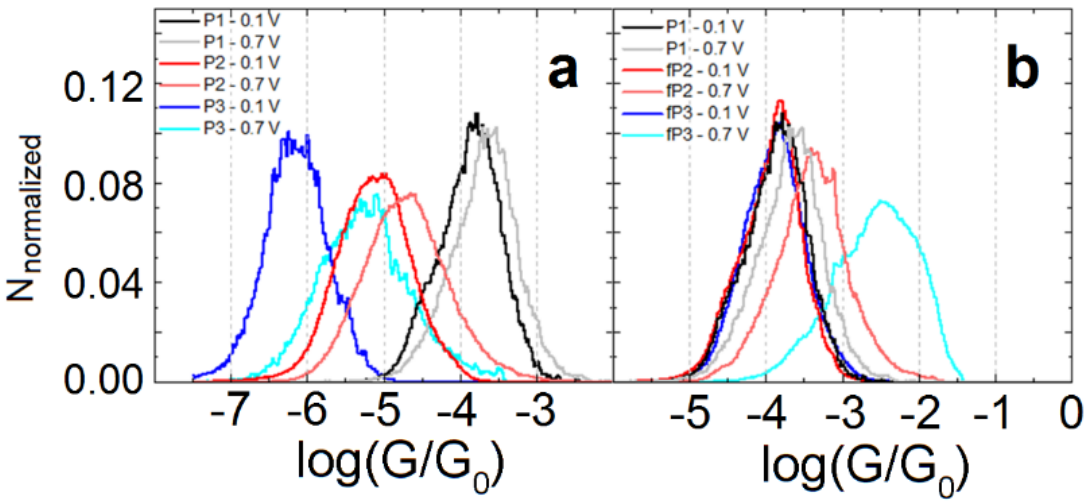

Figure 4.3.1: (a and b) 1D conductance histograms constructed from the data obtained at 0.1 V and 0.7 V for **P1**, **P2**, **P3** and **P1**, **fP2**, **fP3** respectively.

To elucidate the underlying transport mechanisms leading to the observed voltage dependence, I used density functional theory combined with the quantum transport code Gollum to compute the conductance versus voltage of both the fused and C4-linked molecules. The resulting transmission curves are shown in Figure (4.3.2, a) and the corresponding conductance versus voltage curves are presented in figures (4.3.2, b). In the case of the fused porphyrins, the Fermi level lies in the tail of their non-degenerate

HOMOs and the HOMO dominated transport is obtained. As expected, the conductance increases with voltage for all molecules. At zero bias, $G_{P3} << G_{P2} << G_{P1}$, whereas for the fused series, the conductance values lie within a factor two of each other, consistent with the experiments Figure (4.3.2, c). As the bias is increased, however, then beyond 0.5 V the following trend is obtained: conductance of $G_{fP3} >> G_{fP2} >> G_{P1}$, which is in stark contrast to the C4-linked series where the behaviour remains $G_{P3} < G_{P2} < G_{P1}$. This again is in good agreement with the experimental values as shown in figure (4.3.2, c).

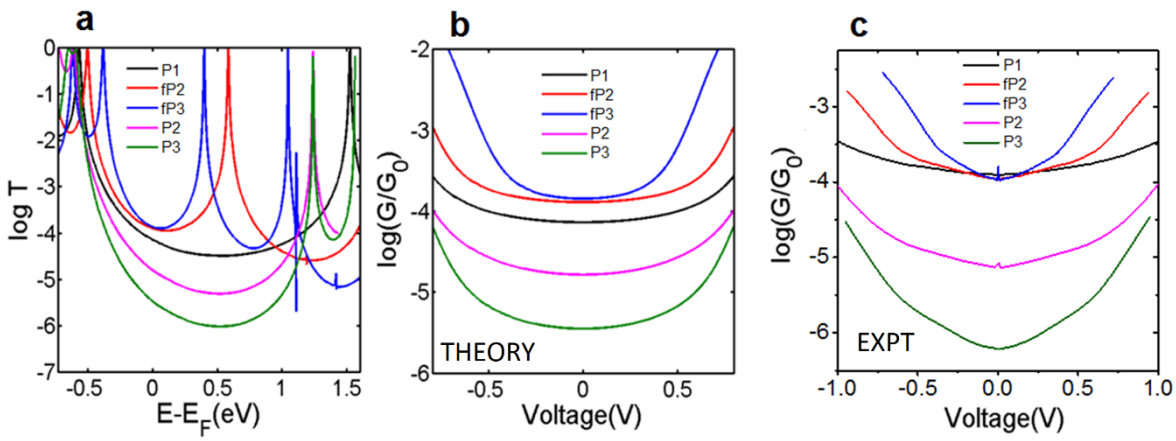

Figure 4.3.2: (a) Calculated transmission coefficient using mean field Hamiltonian obtained from DFT for fused and butadiyne-linked porphyrin series. (b) Calculated conductance vs. bias voltage for each compound (c) Mean experimental $\log(G/G_0)$ traces for each compound.

Bibliography

(1) Scholes, G. D.; Fleming, G. R.; Olaya-Castro, A.; Van Grondelle, R. Lessons from Nature about Solar Light Harvesting. *Nat. Chem.* **2011**, *3* (10), 763.

(2) Ruiz, M. P.; Aragonès, A. C.; Camarero, N.; Vilhena, J. G.; Ortega, M.; Zotti, L. A.; Perez, R.; Cuevas, J. C.; Gorostiza, P.; D\'\iez-Pérez, I. Bioengineering a Single-Protein Junction. *J. Am. Chem. Soc.* **2017**, *139* (43), 15337–15346.

(3) Amdursky, N.; Marchak, D.; Sepunaru, L.; Pecht, I.; Sheves, M.; Cahen, D. Electronic Transport via Proteins. *Adv. Mater.* **2014**, *26* (42), 7142–7161.

(4) Li, Z.; Li, H.; Chen, S.; Froehlich, T.; Yi, C.; Schonenberger, C.; Calame, M.; Decurtins, S.; Liu, S.-X.; Borguet, E. Regulating a Benzodifuran Single Molecule Redox Switch via Electrochemical Gating and Optimization of Molecule/Electrode Coupling. *J. Am. Chem. Soc.* **2014**, *136* (25), 8867–8870.

(5) Kim, Y.; Hellmuth, T. J.; Sysoiev, D.; Pauly, F.; Pietsch, T.; Wolf, J.; Erbe, A.; Huhn, T.; Groth, U.; Steiner, U. E.; et al. Charge Transport Characteristics of Diarylethene Photoswitching Single-Molecule Junctions. *Nano Lett.* **2012**, *12* (7), 3736–3742.

(6) Frisbie, C. D. Designing a Robust Single-Molecule Switch. *Science (80-.).* **2016**, *352* (6292), 1394–1395.

(7) Darwish, N.; Diez-Perez, I.; Guo, S.; Tao, N.; Gooding, J. J.; Paddon-Row, M. N. Single Molecular Switches: Electrochemical Gating of a Single Anthraquinone-Based Norbornylogous Bridge Molecule. *J. Phys. Chem. C* **2012**, *116* (39), 21093–21097.

(8) Zhou, J.; Wang, K.; Xu, B.; Dubi, Y. Photoconductance from Exciton Binding in

Molecular Junctions. *J. Am. Chem. Soc.* **2017**, *140* (1), 70–73.

(9) Evangeli, C.; Gillemot, K.; Leary, E.; Gonzalez, M. T.; Rubio-Bollinger, G.; Lambert, C. J.; Agra\"\it, N. Engineering the Thermopower of C60 Molecular Junctions. *Nano Lett.* **2013**, *13* (5), 2141–2145.

(10) Rincón-Garc\'\ia, L.; Evangeli, C.; Rubio-Bollinger, G.; Agra\"\it, N. Thermopower Measurements in Molecular Junctions. *Chem. Soc. Rev.* **2016**, *45* (15), 4285–4306.

(11) Cui, L.; Miao, R.; Wang, K.; Thompson, D.; Zotti, L. A.; Cuevas, J. C.; Meyhofer, E.; Reddy, P. Peltier Cooling in Molecular Junctions. *Nat. Nanotechnol.* **2018**, *13* (2), 122.

(12) Sedghi, G.; García-Suárez, V. M.; Esdaile, L. J.; Anderson, H. L.; Lambert, C. J.; Martín, S.; Bethell, D.; Higgins, S. J.; Elliott, M.; Bennett, N.; et al. Long-Range Electron Tunnelling in Oligo-Porphyrin Molecular Wires. *Nat. Nanotechnol.* **2011**, *6* (8), 517–523.

(13) Sedghi, G.; Esdaile, L. J.; Anderson, H. L.; Martin, S.; Bethell, D.; Higgins, S. J.; Nichols, R. J. Comparison of the Conductance of Three Types of Porphyrin-Based Molecular Wires: ??,Meso,??-Fused Tapes, Meso-Butadiyne-Linked and Twisted Meso-Meso Linked Oligomers. *Adv. Mater.* **2012**, *24* (5), 653–657.

(14) Luo, L.; Choi, S. H.; Frisbie, C. D. Probing Hopping Conduction in Conjugated Molecular Wires Connected to Metal Electrodes. *Chem. Mater.* **2010**, *23* (3), 631–645.

(15) Winters, M. U.; Dahlstedt, E.; Blades, H. E.; Wilson, C. J.; Frampton, M. J.; Anderson, H. L.; Albinsson, B. Probing the Efficiency of Electron Transfer

through Porphyrin-Based Molecular Wires. *J. Am. Chem. Soc.* **2007**, *129* (14), 4291–4297.

(16) Kuang, G.; Chen, S. Z.; Yan, L.; Chen, K. Q.; Shang, X.; Liu, P. N.; Lin, N. Negative Differential Conductance in Polyporphyrin Oligomers with Nonlinear Backbones. *J. Am. Chem. Soc.* **2018**, *140* (2), 570–573.

(17) Li, Z.; Park, T. H.; Rawson, J.; Therien, M. J.; Borguet, E. Quasi-Ohmic Single Molecule Charge Transport through Highly Conjugated Meso-to-Meso Ethyne-Bridged Porphyrin Wires. *Nano Lett.* **2012**, *12* (6), 2722–2727.

(18) Tanaka, T.; Osuka, A. Conjugated Porphyrin Arrays: Synthesis, Properties and Applications for Functional Materials. *Chem. Soc. Rev.* **2015**, *44* (4), 943–969.

(19) Li, Z.; Smeu, M.; Ratner, M. A.; Borguet, E. Effect of Anchoring Groups on Single Molecule Charge Transport through Porphyrins. *J. Phys. Chem. C* **2013**, *117* (29), 14890–14898.

(20) Kiguchi, M.; Takahashi, T.; Kanehara, M.; Teranishi, T.; Murakoshi, K. Effect of End Group Position on the Formation of a Single Porphyrin Molecular Junction. *J. Phys. Chem. C* **2009**, *113* (21), 9014–9017.

(21) Perrin, M. L.; Verzijl, C. J. O.; Martin, C. a.; Shaikh, A. J.; Eelkema, R.; Esch, J. H. Van; van Ruitenbeek, J. M.; Thijssen, J. M.; van der Zant, H. S. J.; Dulić, D.; et al. Large Tunable Image-Charge Effects in Single-Molecule Junctions. *Nat. Nanotechnol.* **2013**, *8* (4), 282–287.

(22) Holten, D.; Bocian, D. F.; Lindsey, J. S. Probing Electronic Communication in Covalently Linked Multiporphyrin Arrays. A Guide to the Rational Design of Molecular Photonic Devices. *Acc. Chem. Res.* **2002**, *35* (1), 57–69.

(23) Anderson, H. L. Conjugated Porphyrin Ladders. *Inorg. Chem.* **1994**, *33* (5), 972–981.

(24) Taylor, P. N.; Huuskonen, J.; Aplin, R. T.; Anderson, H. L.; Rumbles, G.; Williams, E. Conjugated Porphyrin Oligomers from Monomer to Hexamer. *Chem. Commun.* **1998**, No. 8, 909–910.

(25) Lin, V. S.; DiMagno, S. G.; Therien, M. J. Highly Conjugated, Acetylenyl Bridged Porphyrins: New Models for Light-Harvesting Antenna Systems. *Science (80-.).* **1994**, *264* (5162), 1105–1111.

(26) Tsuda, A.; Osuka, A. Fully Conjugated Porphyrin Tapes with Electronic Absorption Bands That Reach into Infrared. *Science (80-.).* **2001**, *293* (5527), 79–82.

(27) Kang, B. K.; Aratani, N.; Lim, J. K.; Kim, D.; Osuka, A.; Yoo, K.-H. Length and Temperature Dependence of Electrical Conduction through Dithiolated Porphyrin Arrays. *Chem. Phys. Lett.* **2005**, *412* (4–6), 303–306.

(28) Algethami, N.; Sadeghi, H.; Sangtarash, S.; Lambert, C. J. The Conductance of Porphyrin-Based Molecular Nanowires Increases with Length. *Nano Lett.* **2018**.

(29) Kuang, G.; Chen, S.-Z.; Wang, W.; Lin, T.; Chen, K.; Shang, X.; Liu, P. N.; Lin, N. Resonant Charge Transport in Conjugated Molecular Wires beyond 10 Nm Range. *J. Am. Chem. Soc.* **2016**, *138* (35), 11140–11143.

(30) Wang, W.; Lee, T.; Reed, M. A. Mechanism of Electron Conduction in Self-Assembled Alkanethiol Monolayer Devices. *Phys. Rev. B* **2003**, *68* (3), 35416.

(31) Koch, M.; Ample, F.; Joachim, C.; Grill, L. Voltage-Dependent Conductance of a Single Graphene Nanoribbon. *Nat. Nanotechnol.* **2012**, *7* (11), 713.

(32) Arroyo, C. R.; Leary, E.; Castellanos-Gómez, A.; Rubio-Bollinger, G.; Gonzalez, M. T.; Agra\"\it, N. Influence of Binding Groups on Molecular Junction Formation. *J. Am. Chem. Soc.* **2011**, *133* (36), 14313–14319.

(33) Li, C.; Pobelov, I.; Wandlowski, T.; Bagrets, A.; Arnold, A.; Evers, F. Charge Transport in Single Au Alkanedithiol Au Junctions: Coordination Geometries and Conformational Degrees of Freedom. *J. Am. Chem. Soc.* **2008**, *130* (1), 318–326.

(34) Venkataraman, L.; Klare, J. E.; Nuckolls, C.; Hybertsen, M. S.; Steigerwald, M. L. Dependence of Single-Molecule Junction Conductance on Molecular Conformation. *Nature* **2006**, *442* (7105), 904.

(35) Kaliginedi, V.; Moreno-García, P.; Valkenier, H.; Hong, W.; García-Suárez, V. M.; Buiter, P.; Otten, J. L. H. H.; Hummelen, J. C.; Lambert, C. J.; Wandlowski, T. Correlations between Molecular Structure and Single-Junction Conductance: A Case Study with Oligo(Phenylene-Ethynylene)-Type Wires. *J. Am. Chem. Soc.* **2012**, *134* (11), 5262–5275.

(36) Soler, J.; Artacho, E.; Gale, J.; Garcia, A.; Junquera, J.; Ordejon, P.; Sanchez-Portal, D. The SIESTA Method for Ab Initio Order-N Materials Simulation. *J. PHYSICS-CONDENSED MATTER* **2002**, *14* (11), 2745–2779.

(37) Ferrer, J.; Lambert, C. J.; García-Suárez, V. M.; Manrique, D. Z.; Visontai, D.; Oroszlany, L.; Rodríguez-Ferradás, R.; Grace, I.; Bailey, S.; Gillemot, K. GOLLUM: A next-Generation Simulation Tool for Electron, Thermal and Spin Transport. *New J. Phys.* **2014**, *16* (9), 093029.

(38) Perdew, J. P.; Burke, K.; Ernzerhof, M. Generalized Gradient Approximation Made Simple. *Phys. Rev. Lett.* **1996**, *77* (18), 3865.

Chapter 5

Cross conjugation increases the conductance of *meta*-connected fluorenones

Charge transport through *meta*-connected biphenylene is strongly suppressed by destructive quantum interference (DQI) and as I demonstrate here in this chapter, this suppression persists when a saturated tetrahedral carbon is added to bridge the biphenyl moiety yielding a fluorene. The results demonstrate that the main effect of the bridge atom is to alleviate the DQI transmission dip from the middle of HOMO and LUMO of the *meta*-connected biphenylene core and increase the conductance of the resulting *meta*-connected fluorene and fluorenone cores. This work was carried out in collaboration with the experimental group in Oxford and Liverpool university. The results presented in this chapter were submitted on Nanoscale.

5.1 Introduction

Molecular-scale electronics[1,2] is a branch of nanoelectronics in which the electrical components are formed from single or a few molecules. The measurement and understanding of charge transport in single molecules are essential for the development of single-molecule electronic devices[3–7]. Several experimental approaches have been established for measuring transport through single (or a few) molecules, notably the mechanically controlled break junction (MCBJ) and scanning tunnelling microscopy-break junction (STM-BJ) techniques[8,9]. Over the last two decades, a variety of anchor groups have been synthesized for binding single molecules to metallic electrodes[5,10], including pyridines[11], amines[12], thiols and methyl sulphides[13,14]. These studies of charge-transport through single molecules trapped between two metallic electrodes demonstrate that anchor groups, molecular lengths, the nature of spacers and electronic structures of the aromatic subunits, can significantly affect transmission through molecular devices[15–18]. Other key factors are the molecular conformation, the gap between the highest occupied and the lowest unoccupied molecular orbitals (the HOMO-LUMO gap)[19,20], the alignment of this gap to the Fermi level of the metal electrodes, and the coordination geometry at the metal-molecule contacts.

Recent studies have also revealed that changing the connectivity to electrodes of phenyl rings from *para* to *meta* reduces their electrical conductance, because it switches the quantum interference (QI) in their π systems from constructive quantum interference (CQI) to destructive quantum interference (DQI)[1,2,21–28]. Here I examine how this transition from CQI to DQI can be controlled by placing bridge atoms across the biphenylene core of oligo(arylene-ethynylene) (OAE)-type molecular wires[29]. Previous studies have shown that *para*-connected cross-conjugated anthraquinone-based molecules have a significantly lower conductance compared to fully conjugated

counterparts[30–34] and that *para*-connected fluorenones exhibit constructive CQI in the HOMO-LUMO gap[35]. Here I study the electrical conductance of a *meta*-connected cross-conjugated core. I demonstrate theoretically that the DQI of the *meta*-connected biphenylene core is alleviated in the *meta*-connected cross conjugated fluorenone, leading to a high conductance, which is comparable with *para*-connected fluorenone. Also the experimental result from our collaborators confirm my calculation and a recent prediction that cross conjugation increases the conductance of *meta*-connected anthraquinone[36].

5.2 Molecular structure

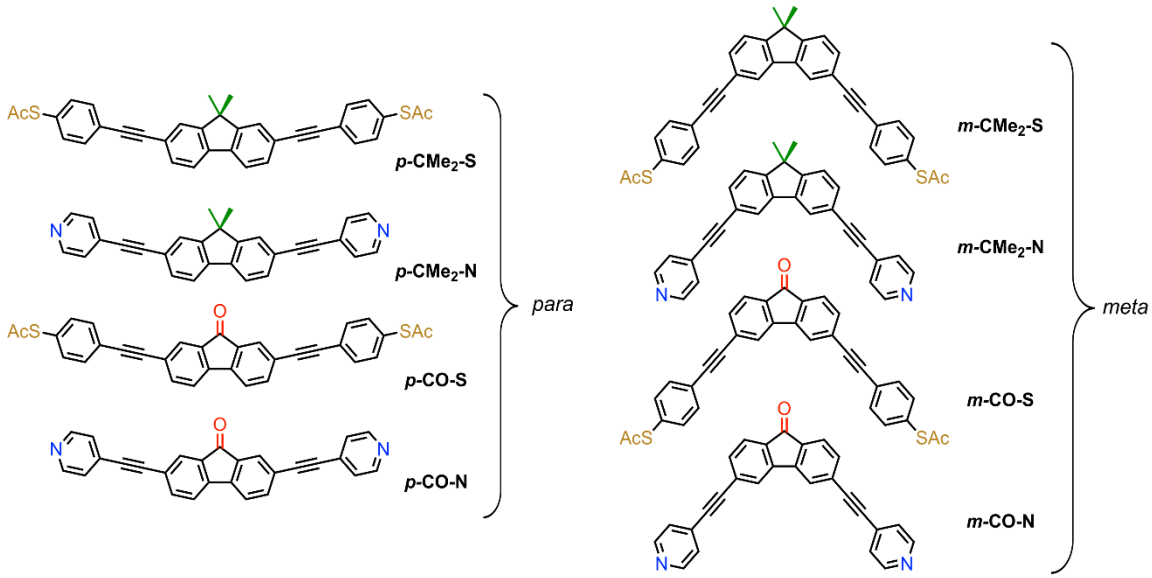

Figure 5.2.1: Chemical structures of the eight compounds investigated.

During this study, the single-molecule conductance of eight compounds with the molecular structures illustrated in figure (5.2.1) is compared: fluorenes ***p*-CMe$_2$-S**, ***m*-CMe$_2$-S**, ***p*-CMe$_2$-N** and ***m*-CMe$_2$-N**, and fluorenones ***p*-CO-S**, ***m*-CO-S**, ***p*-CO-N** and ***m*-CO-N**.

The optimized geometry and ground state Hamiltonian and overlap matrix elements of each structure were self-consistently obtained using the SIESTA[37] implementation of density functional theory (DFT). SIESTA employs norm-conserving pseudo-potentials to account for the core electrons and linear combinations of atomic orbitals to construct the valence states. The generalized gradient approximation (GGA) of the exchange and correlation functional is used with the Perdew-Burke-Ernzerhof parameterization (PBE)[38], a double-ζ polarized (DZP) basis set, a real-space grid defined with an equivalent energy cut-off of 250 Ry. The geometry optimization for each structure is performed to the forces smaller than 10 meV/Å. Figures (5.2.2) and (5.2.3) show geometry-optimized structures used to obtain the DFT results. The mean-field Hamiltonian obtained from the converged DFT calculation or a simple tight-binding Hamiltonian was combined with our Gollum quantum transport code[39] to calculate the phase-coherent, elastic scattering properties of each system consist of left (source) and right (drain) leads and the scattering region.

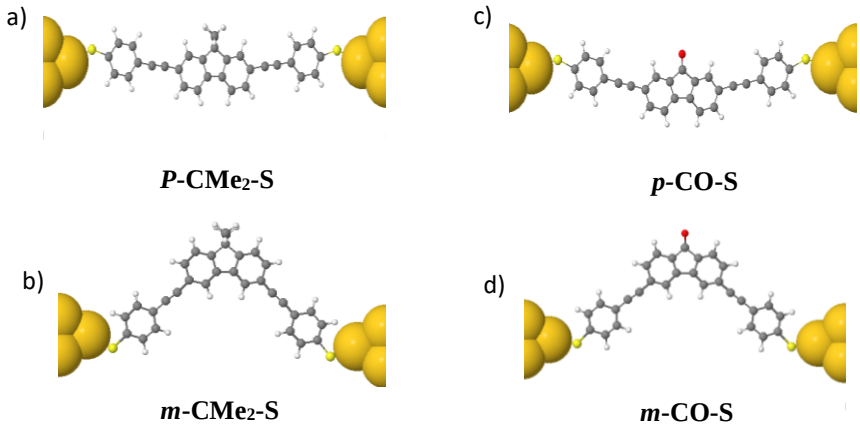

Figure 5.2.2: Relaxed structure of: (a),(b) fluorene core connected to thiol anchor using *para* and *meta* connectivity, (c),(d) fluorenone core connected to thiol anchor using *para* and *meta* connectivity.

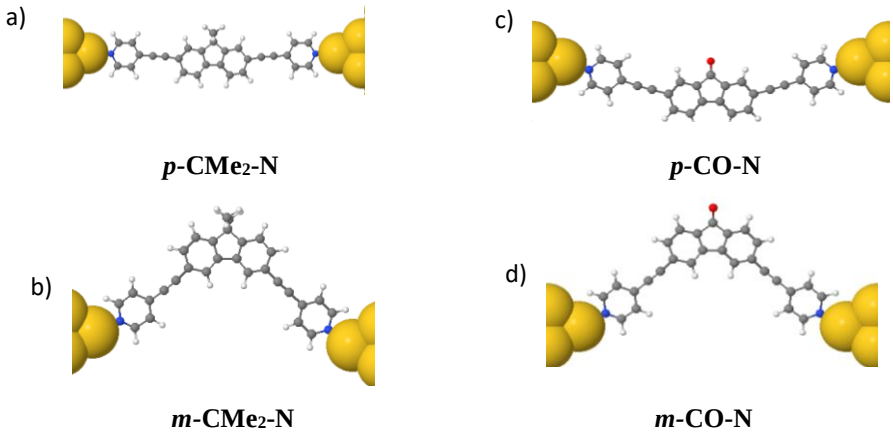

Figure 5.2.3: Relaxed structure of: (a), (b) fluorene core connected to pyridine anchor using *para* and *meta* connectivity, (c), (d) fluorenone core connected to pyridine anchor using *para*- and *meta*- connectivity.

5.3 Results and discussion

The most surprising outcome is that for the *meta*-compounds with both thiol and pyridyl anchor groups, replacing the CMe_2 bridge by a C=O leads to a dramatic increase in conductance, close to a factor 30. The same replacement in the *para*-compounds has a negligible influence (both *p*-CO compounds actually appear to be fractionally lower in conductance than the *p*-CMe_2 counterparts). This agrees with previous results on *para*-connected OPE3 molecules where different substituents on the central phenyl ring have a negligible effect on conductance[22,23,40]. Viewed another way, switching from *para* to *meta* connectivity when the bridge is CMe_2 causes the conductance to drop two orders of magnitude. In contrast, when the bridge is C=O, the same operation causes the conductance to drop by only a factor 2-3. This behavior is remarkable, because from a valence-bond perspective, each terminal S/N atom is formally cross-conjugated via the carbonyl group, as noted for similar structures by Estrada et al. and Homnick et al[41,42], and as such no direct alternating single/double bond path exists for *meta*-connectivity. Comparing the thiols and the pyridyls more generally, for any given backbone, the conductance is always about 10 times lower for pyridyls compared to thiols. There are not many published reports directly comparing thiol anchors with pyridyls. In reference[43]exchanged the benzenethiol, PhS, groups in an OPE3 wire for Py resulting in a 30-fold drop in conductance. In two separate studies[44,45] 1,4-bis-4,4'-pyridyl benzene was measured to have a conductance of $\log(G/G_0) = -4.7$, whereas *p*-terphenyl dithiol was measured at $\log(G/G_0) = -3.2$ (also about a factor 30 difference). These results are, therefore, consistent with the previous results in displaying about an order of magnitude drop in conductance when exchanging PhS with Py.

Figure (5.3.1) below shows the calculated conductance of the molecules in *para* and *meta* connectivities for fluorene and fluorenone with thiol (a and c) and pyridine anchors (b and d) respectively for the relaxed structure of the molecules between leads have been shown in Figure (5.2.2) and (5.2.3). For comparison, the horizontal bands in show the measured conductance values in the second column of Table (5.3.1). The widths of the horizontal bands correspond to the experimental full width at half maximum (FWHM) of a conductance peak.

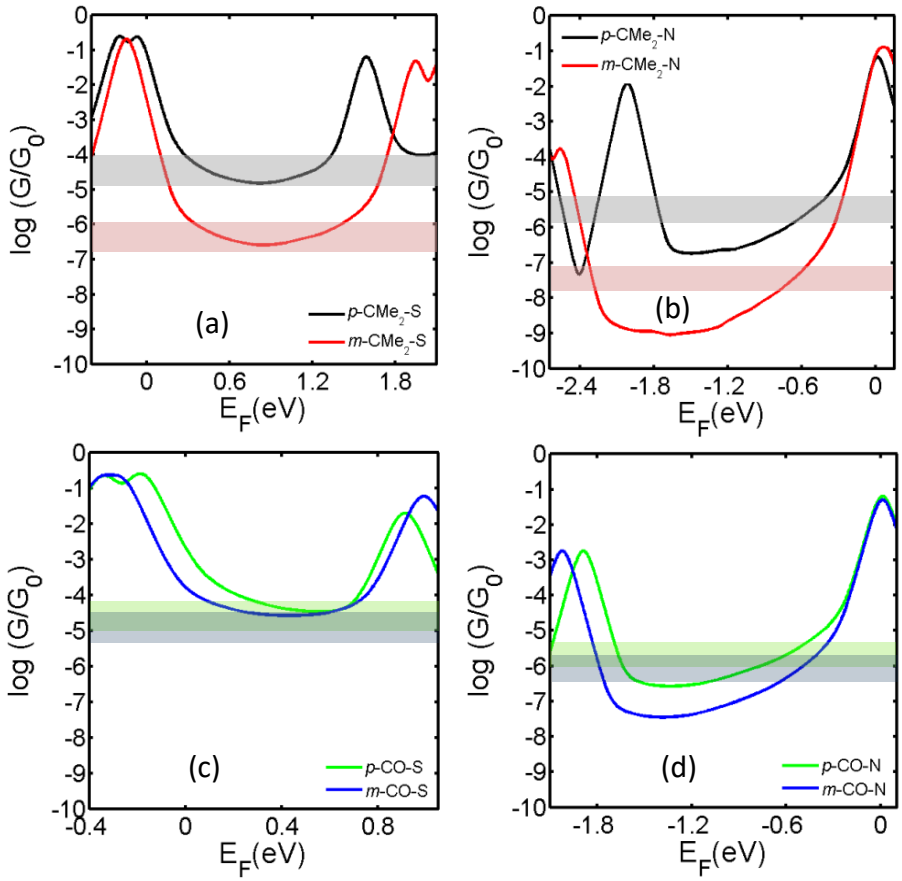

Figure 5.3.1: The calculated room-temperature conductances of (a) ***p*-CMe$_2$-S** and ***m*-CMe$_2$-S**; (b) ***p*-CMe$_2$-N** and ***m*-CMe$_2$-N**; (c) ***p*-CO-S** and ***m*-CO-S**; (d) ***p*-CO-N** and ***m*-CO-N**; connected to gold electrodes, obtained from DFT. Results are plotted against the Fermi energy E_F, where $E_F = 0$ corresponds to the DFT-predicted Fermi energy. For comparison, the horizontal bands show the measured conductance values in the second column of Table (5.3.1). The widths of the horizontal bands are equal to the FWHM quoted in the second column of Table (5.3.1).

As illustrated in figure (5.3.1) for a range of Fermi energies between the HOMO and LUMO resonances there is qualitative agreement between calculated and measured conductance trends of the molecules shows in figure (5.3.2). For both thiol and pyridyl anchors, there is a large ratio (about 2 orders of magnitude) between the conductances of *para vs. meta* connected fluorene molecules and a significantly smaller ratio between the conductance of the *para* and *meta* connected fluorenones. The magnitude of the conductance with pyridyl anchors is about one order of magnitude lower than with thiol anchors. Furthermore, the conductance of the *meta*-connected fluorenone with thiol anchors is surprisingly high. From these results, I conclude that the bridge atom strongly enhances the conductance of the *meta* connected molecules but does not significantly influence *para*-connected molecules.

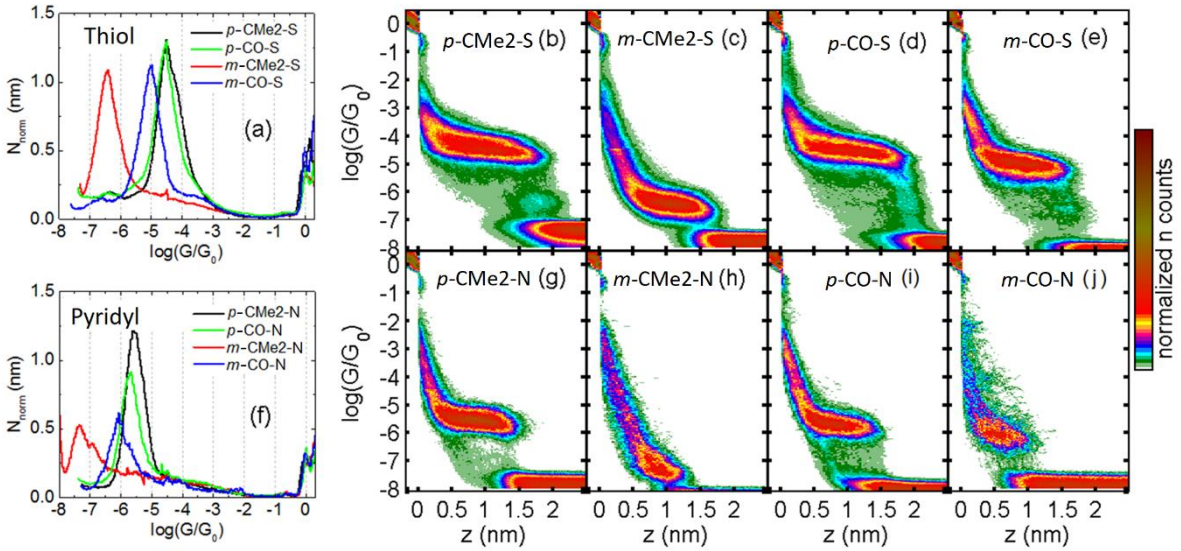

Figure 5.3.2: (a/f) 1D conductance histograms for thiol/pyridyls-terminated compounds respectively. (b-e/g-j) $\log(G/G_0)$-z 2D histograms generated from all plateau-containing traces for thiol/pyridyl terminated compounds. N_{junc} = 6486 (68 %) (***p*-CMe$_2$-S**), 6180 (49 %) (***m*-CMe$_2$-S**), 4881 (52 %) (***p*-CO-S**), 2318 (30 %) (***m*-CO-S**), 1600 (40 %) (***p*-CMe$_2$-N**), 579 (39 %) (***m*-CMe$_2$-N**), 1517 (17 %) (***p*-CO-N**), 310 (9 %) (***m*-CO-N**).

The DFT-predicted HOMO-LUMO gaps in Table (5.3.1) show that there is a correlation between HOMO-LUMO gaps and the measured conductances. When switching from *para* to *meta* connectivity, the HOMO-LUMO gaps always increase. However, the increase is small for the fluorenones and significantly larger for the fluorenes. This correlates with the smaller reduction in conductance for the fluorenone core compared with fluorene and can be attributed to conjugation between the anchor groups and the C=O in the *meta*-fluorenones. However, the gap for *para*-fluorenes is always larger than the corresponding *meta*-fluorenones, yet the conductance is lower for the *meta*-fluorenones than the *para*-fluorenes. This demonstrates that HOMO-LUMO gaps are not absolute predictors of molecular conductance, and that the quantum interference due to scattering from the bridge atom(s) plays a significant role.

Molecule	Measured low-bias Conductance ($\log(G/G_0)$)	Measured 95th percentile (L_{95}) + 0.4 nm	Theoretical Au-Au distance (nm)	DFT-predicted HOMO-LUMO gaps (eV)
***p*-CMe$_2$-S**	-4.5 (0.9)	2.6	2.5	2.13
***m*-CMe$_2$-S**	-6.4 (0.8)	2.4	2.2	2.63
***p*-CO-S**	-4.6 (0.8)	2.6	2.5	1.65
***m*-CO-S**	-5.0 (0.8)	2.3	2.2	1.81
***p*-CMe$_2$-N**	-5.6 (0.7)	2.2	2.4	2.30
***m*-CMe$_2$-N**	-7.4 (0.6)	1.9	1.8	2.95
***p*-CO-N**	-5.7 (0.6)	2.2	2.4	1.96
***m*-CO-N**	-6.1 (0.7)	1.7	1.8	2.08

Table (5.3.1): Measured low-bias single molecule conductance values and junction length data. The values in parentheses are the FWHM. The Au-Au distance is the calculated separation between two gold atoms attached to the two terminal S/N atoms of the extended molecules, from the calculated molecular geometry.

To further investigate the effect of the bridge I have also examined the conductance ratio of biphenylene with para and meta connectivities as shown in figure (5.3.3). As it is clear in this figure there is no conjugation path between two biphenyls and therefore the destructive interference with meta connectivity is more pronounce and as predicted, the value of transmission coefficient of the para connectivitiy is very similar to the fluorene and fluorenone cores, which confirming our prediction that changing the bridge between two phenyl rings has no effect on para connectivity. for comparison I have shown the conductance of para and meta of all the molecules in figure (5.3.4).

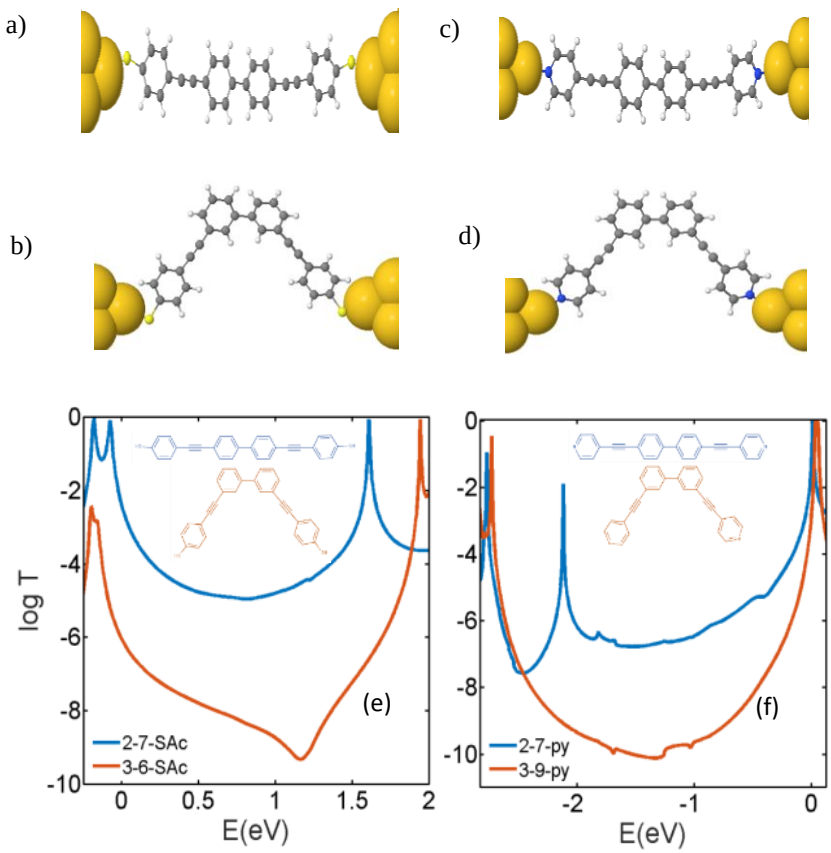

Figure (5.3.3): Relaxed structure of: (a, b) biphenyl core connected to thiol anchor using *para* and *meta* connectivity, (c, d) biphenyl core connected to pyridine anchor using *para* and *meta* connectivity. (e) Transmission coefficient of *para* connectivities (blue) and (red) for *meta* connectivities of biphenyl with thiol anchor. (f) conductance of *para* connectivities (blue) and (red) for *meta* connectivities of biphenyl with pyridine anchor.

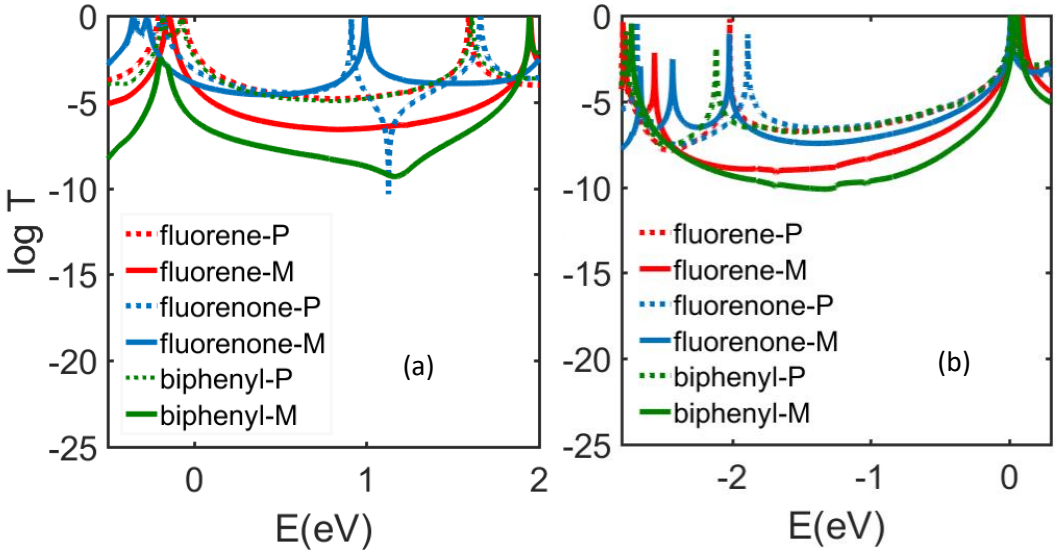

Figure (5.3.4): (a) conductance of *para* connectivities (dashed-line) and (solid-line) for *meta* connectivities for fluorene, fluorenone and biphenyl with thiol anchor. (b) conductance of *para* connectivities (dashed-line) and (solid-line) for *meta* connectivities for fluorene, fluorenone and biphenyl with pyridine anchor.

To demonstrate the role of the bridge in the core of the molecule, I consider the series of tight binding models figure (5.3.5, a), where only nearest neighbor couplings between π-orbitals are included. The energy scale and energy origin are fixed by choosing the nearest neighbor couplings to be unity and all site energies to be zero except for the energy ε_9 of site number 9. For modeling a biphenyl bridge, site 9 is absent. For modeling the fluorenone, ε_9 is equal to 1.7 and for the fluorene ε_9 is equal to 5. The qualitative agreement between the material-specific results of figure (5.3.1) and the tight-binding results of figure (5.3.5, b, c and d) demonstrates that the main effect of the bridge atom is to alleviate the DQI transmission dip from the middle of HOMO and LUMO of the meta-connected biphenylene core and increase the conductance of the resulting meta-connected fluorene and fluorenone cores.

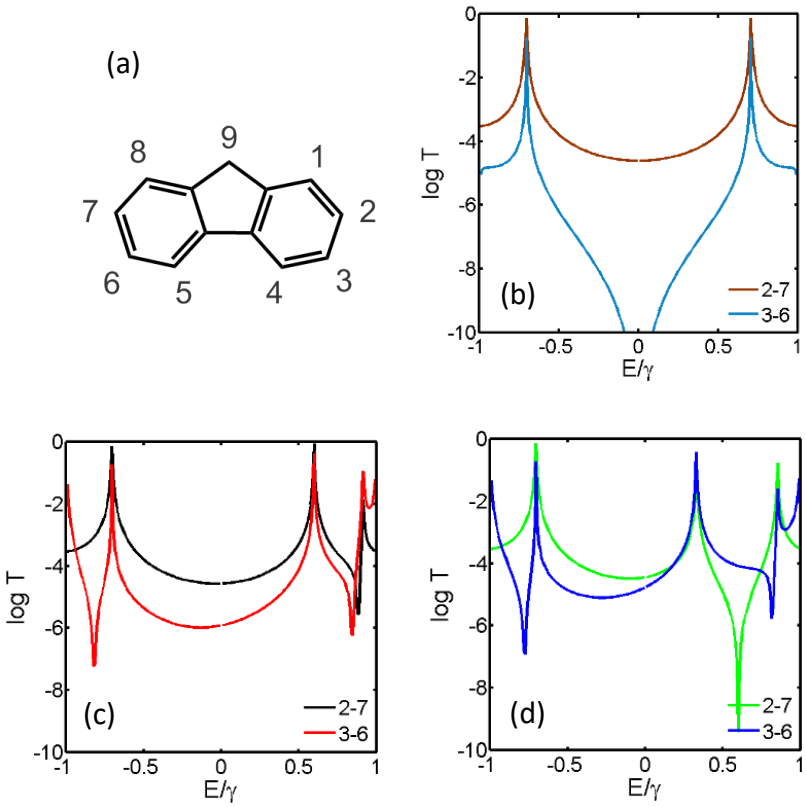

Figure 5.3.5: (a) Numbering system and structure considered in the TB model. (b) The transmission coefficients for biphenyl in *para* (2-7) and *meta* (3-6), (c) fluorene in *para* (2-7) and *meta* (3-6), (d) fluorenone in *para* (2-7) and *meta* (3-6) position. The value of ε_9 are 5 and 1.7 in c and d respectively.

Bibliography

(1) Briere, J.-F.; Côté, M. Electronic, Structural, and Optical Properties of Conjugated Polymers Based on Carbazole, Fluorene, and Borafluorene. *J. Phys. Chem. B* **2004**, *108* (10), 3123–3129.

(2) Lambert, C. J. Basic Concepts of Quantum Interference and Electron Transport in Single-Molecule Electronics. *Chem. Soc. Rev.* **2015**, *44* (4), 875–888.

(3) Sadeghi, H. Theory of Electron, Phonon and Spin Transport in Nanoscale Quantum Devices. *Nanotechnology* **2018**.

(4) Elke, S.; Carlos, C. J. *Molecular Electronics: An Introduction to Theory and Experiment*; World Scientific, 2017; Vol. 15.

(5) Leary, E.; La Rosa, A.; González, M. T.; Rubio-Bollinger, G.; Agra\"\it, N.; Mart\’\in, N. Incorporating Single Molecules into Electrical Circuits. The Role of the Chemical Anchoring Group. *Chem. Soc. Rev.* **2015**, *44* (4), 920–942.

(6) Perrin, M. L.; Burzur\’\i, E.; van der Zant, H. S. J. Single-Molecule Transistors. *Chem. Soc. Rev.* **2015**, *44* (4), 902–919.

(7) Chen, F.; Hihath, J.; Huang, Z.; Li, X.; Tao, N. J. Measurement of Single-Molecule Conductance. *Annu. Rev. Phys. Chem.* **2007**, *58*, 535–564.

(8) Nichols, R. J.; Higgins, S. J. Single Molecule Nanoelectrochemistry in Electrical Junctions. *Acc. Chem. Res.* **2016**, *49* (11), 2640–2648.

(9) Schwarz, F.; Lörtscher, E. Break-Junctions for Investigating Transport at the Molecular Scale. *J. Phys. Condens. Matter* **2014**, *26* (47), 474201.

(10) Wang, L.; Wang, L.; Zhang, L.; Xiang, D. Advance of Mechanically Controllable Break Junction for Molecular Electronics. In *Molecular-Scale Electronics*; Springer, 2019; pp 45–86.

(11) Hong, W.; Manrique, D. Z.; Moreno-Garcia, P.; Gulcur, M.; Mishchenko, A.;

Lambert, C. J.; Bryce, M. R.; Wandlowski, T. Single Molecular Conductance of Tolanes: Experimental and Theoretical Study on the Junction Evolution Dependent on the Anchoring Group. *J. Am. Chem. Soc.* **2012**, *134* (4), 2292–2304.

(12) Chen, F.; Li, X.; Hihath, J.; Huang, Z.; Tao, N. Effect of Anchoring Groups on Single-Molecule Conductance: Comparative Study of Thiol-, Amine-, and Carboxylic-Acid-Terminated Molecules. *J. Am. Chem. Soc.* **2006**, *128* (49), 15874–15881.

(13) Wu, S.; González, M. T.; Huber, R.; Grunder, S.; Mayor, M.; Schönenberger, C.; Calame, M. Molecular Junctions Based on Aromatic Coupling. *Nat. Nanotechnol.* **2008**, *3* (9), 569.

(14) Sangtarash, S.; Vezzoli, A.; Sadeghi, H.; Ferri, N.; Brien, H. M. O. Gateway State-Mediated, Long-Range Tunnelling in Molecular Wires. 1 , 2. *Nanoscale* **2018**, *10*, 3060–3067. https://doi.org/10.17638/datacat.liverpool.ac.uk/198.3.

(15) Sendler, T.; Luka-Guth, K.; Wieser, M.; Wolf, J.; Helm, M.; Gemming, S.; Kerbusch, J.; Scheer, E.; Huhn, T.; Erbe, A. Light-Induced Switching of Tunable Single-Molecule Junctions. *Adv. Sci.* **2015**, *2* (5), 1500017.

(16) Perrin, M. L.; Galán, E.; Eelkema, R.; Thijssen, J. M.; Grozema, F.; van der Zant, H. S. J. A Gate-Tunable Single-Molecule Diode. *Nanoscale* **2016**, *8* (16), 8919–8923.

(17) Huang, C.; Chen, S.; Ørnsø, K. B.; Reber, D.; Baghernejad, M.; Fu, Y.; Wandlowski, T.; Decurtins, S.; Hong, W.; Thygesen, K. S.; et al. Controlling Electrical Conductance through a $π$-Conjugated Cruciform Molecule by Selective Anchoring to Gold Electrodes. *Angew. Chemie Int. Ed.* **2015**, *54* (48), 14304–14307.

(18) Bai, J.; Daaoub, A.; Sangtarash, S.; Li, X.; Tang, Y.; Zou, Q.; Sadeghi, H.; Liu,

S.; Huang, X.; Tan, Z.; et al. Anti-Resonance Features of Destructive Quantum Interference in Single-Molecule Thiophene Junctions Achieved by Electrochemical Gating. *Nat. Mater.* **2019**, 1.

(19) Leary, E.; Limburg, B.; Alanazy, A.; Sangtarash, S.; Grace, I.; Swada, K.; Esdaile, L. J.; Noori, M.; Gonzalez, M. T.; Rubio-Bollinger, G.; et al. Bias-Driven Conductance Increase with Length in Porphyrin Tapes. *J. Am. Chem. Soc.* **2018**, *140* (40), 12877–12883.

(20) Algethami, N.; Sadeghi, H.; Sangtarash, S.; Lambert, C. J. The Conductance of Porphyrin-Based Molecular Nanowires Increases with Length. *Nano Lett.* **2018**.

(21) Yang, Y.; Gantenbein, M.; Alqorashi, A.; Wei, J.; Sangtarash, S.; Hu, D.; Sadeghi, H.; Zhang, R.; Pi, J.; Chen, L.-C.; et al. Heteroatom-Induced Molecular Asymmetry Tunes Quantum Interference in Charge Transport through Single-Molecule Junctions. *J. Phys. Chem. C* **2018**.

(22) Liu, X.; Sangtarash, S.; Reber, D.; Zhang, D.; Sadeghi, H.; Shi, J.; Xiao, Z.-Y.; Hong, W.; Lambert, C. J.; Liu, S.-X. Gating of Quantum Interference in Molecular Junctions by Heteroatom Substitution. *Angew. Chemie Int. Ed.* **2017**, *56* (1), 173–176.

(23) Sangtarash, S.; Sadeghi, H.; Lambert, C. J. Exploring Quantum Interference in Heteroatom-Substituted Graphene-like Molecules. *Nanoscale* **2016**, *8* (27), 13199–13205.

(24) Sangtarash, S.; Huang, C.; Sadeghi, H.; Sorohhov, G.; Hauser, J.; Wandlowski, T.; Hong, W.; Decurtins, S.; Liu, S.-X.; Lambert, C. J. Searching the Hearts of Graphene-like Molecules for Simplicity, Sensitivity, and Logic. *J. Am. Chem. Soc.* **2015**, *137* (35), 11425–11431.

(25) Geng, Y.; Sangtarash, S.; Huang, C.; Sadeghi, H.; Fu, Y.; Hong, W.; Wandlowski,

T.; Decurtins, S.; Lambert, C. J.; Liu, S.-X. Magic Ratios for Connectivity-Driven Electrical Conductance of Graphene-like Molecules. *J. Am. Chem. Soc.* **2015**, *137* (13), 4469–4476.

(26) Arroyo, C. R. CR Arroyo, S. Tarkuc, R. Frisenda, JS Seldenthuis, CHM Woerde, R. Eelkema, FC Grozema, and HSJ van Der Zant, Angew. Chem. Int. Ed. 52, 3152 (2013). *Angew. Chem. Int. Ed.* **2013**, *52*, 3152.

(27) Sangtarash, S. Theory of Mid-Gap Quantum Transport through Single Molecule: New Approach to Transport Modeling of Nanoelectronic Devices, Lancaster University, 2017.

(28) Sangtarash, S.; Sadeghi, H.; Lambert, C. J. Connectivity-Driven Bi-Thermoelectricity in Heteroatom-Substituted Molecular Junctions. *Phys. Chem. Chem. Phys.* **2018**, *20* (14), 9630–9637.

(29) Jenny, N. M.; Mayor, M.; Eaton, T. R. Phenyl--Acetylene Bond Assembly: A Powerful Tool for the Construction of Nanoscale Architectures. *European J. Org. Chem.* **2011**, *2011* (26), 4965–4983.

(30) Kaliginedi, V.; Moreno-García, P.; Valkenier, H.; Hong, W.; García-Suárez, V. M.; Buiter, P.; Otten, J. L. H. H.; Hummelen, J. C.; Lambert, C. J.; Wandlowski, T. Correlations between Molecular Structure and Single-Junction Conductance: A Case Study with Oligo(Phenylene-Ethynylene)-Type Wires. *J. Am. Chem. Soc.* **2012**, *134* (11), 5262–5275. https://doi.org/10.1021/ja211555x.

(31) Garc\'\ia, R.; Herranz, M. Á.; Leary, E.; González, M. T.; Bollinger, G. R.; Bürkle, M.; Zotti, L. A.; Asai, Y.; Pauly, F.; Cuevas, J. C.; et al. Supporting Information Single-Molecule Conductance of a Chemically Modified, $π$-Extended Tetrathiafulvalene and Its Charge-Transfer Complex with F 4 TCNQ. *Beilstein J. Org. Chem* **2015**, *11*, 1068–1078.

(32) Guédon, C. M.; Valkenier, H.; Markussen, T.; Thygesen, K. S.; Hummelen, J. C.; Van Der Molen, S. J. Observation of Quantum Interference in Molecular Charge Transport. *Nat. Nanotechnol.* **2012**, *7* (5), 305.

(33) Hong, W.; Valkenier, H.; Mészáros, G.; Manrique, D. Z.; Mishchenko, A.; Putz, A.; Garc\'\ia, P. M.; Lambert, C. J.; Hummelen, J. C.; Wandlowski, T. An MCBJ Case Study: The Influence of $π$-Conjugation on the Single-Molecule Conductance at a Solid/Liquid Interface. *Beilstein J. Nanotechnol.* **2011**, *2*, 699.

(34) Carlotti, M.; Soni, S.; Kumar, S.; Ai, Y.; Sauter, E.; Zharnikov, M.; Chiechi, R. C. Two-Terminal Molecular Memory through Reversible Switching of Quantum Interference Features in Tunneling Junctions. *Angew. Chemie Int. Ed.* **2018**, *57* (48), 15681–15685.

(35) Ashwell, G. J.; Urasinska, B.; Wang, C.; Bryce, M. R.; Grace, I.; Lambert, C. J. Single-Molecule Electrical Studies on a 7 Nm Long Molecular Wire. *Chem. Commun. (Camb).* **2006**, No. 45, 4706–4708. https://doi.org/10.1039/b613347a.

(36) Alqahtani, J.; Sadeghi, H.; Sangtarash, S.; Lambert, C. J. Breakdown of Curly Arrow Rules in Anthraquinone. *Angew. Chemie* **2018**.

(37) Soler, J. M.; Artacho, E.; Gale, J. D.; Garc\'\ia, A.; Junquera, J.; Ordejón, P.; Sánchez-Portal, D. The SIESTA Method for Ab Initio Order-N Materials Simulation. *J. Phys. Condens. Matter* **2002**, *14* (11), 2745.

(38) Perdew, J. P.; Burke, K.; Ernzerhof, M. Generalized Gradient Approximation Made Simple. *Phys. Rev. Lett.* **1996**, *77* (18), 3865.

(39) Ferrer, J.; Lambert, C. J.; García-Suárez, V. M.; Manrique, D. Z.; Visontai, D.; Oroszlany, L.; Rodríguez-Ferradás, R.; Grace, I.; Bailey, S. W. D.; Gillemot, K.; et al. GOLLUM: A next-Generation Simulation Tool for Electron, Thermal and Spin Transport. *New J. Phys.* **2014**, *16*, 093029. https://doi.org/10.1088/1367-

2630/16/9/093029.

(40) Gonzalez, M. T.; Zhao, X.; Manrique, D. Z.; Miguel, D.; Leary, E.; Gulcur, M.; Batsanov, A. S.; Rubio-Bollinger, G.; Lambert, C. J.; Bryce, M. R.; et al. Structural versus Electrical Functionalization of Oligo (Phenylene Ethynylene) Diamine Molecular Junctions. *J. Phys. Chem. C* **2014**, *118* (37), 21655–21662.

(41) Estrada, L. A.; Neckers, D. C. Synthesis and Photophysics of Ambipolar Fluoren-9-Ylidene Malononitrile Derivatives. *J. Org. Chem.* **2009**, *74* (21), 8484–8487.

(42) Homnick, P. J.; Tinkham, J. S.; Devaughn, R.; Lahti, P. M. Engineering Frontier Energy Levels in Donor--Acceptor Fluoren-9-Ylidene Malononitriles versus Fluorenones. *J. Phys. Chem. A* **2013**, *118* (2), 475–486.

(43) Grunder, S.; Huber, R.; Wu, S.; Schönenberger, C.; Calame, M.; Mayor, M. Oligoaryl Cruciform Structures as Model Compounds for Coordination-Induced Single-Molecule Switches. *European J. Org. Chem.* **2010**, *2010* (5), 833–845.

(44) Leary, E.; Zotti, L. A.; Miguel, D.; Márquez, I. R.; Palomino-Ruiz, L.; Cuerva, J. M.; Rubio-Bollinger, G.; González, M. T.; Agrait, N. The Role of Oligomeric Gold--Thiolate Units in Single-Molecule Junctions of Thiol-Anchored Molecules. *J. Phys. Chem. C* **2018**, *122* (6), 3211–3218.

(45) Kamenetska, M.; Quek, S. Y.; Whalley, A. C.; Steigerwald, M. L.; Choi, H. J.; Louie, S. G.; Nuckolls, C.; Hybertsen, M. S.; Neaton, J. B.; Venkataraman, L. Conductance and Geometry of Pyridine-Linked Single-Molecule Junctions. *J. Am. Chem. Soc.* **2010**, *132* (19), 6817–6821.

Chapter 6

Conclusion and future work

6.1 Conclusion

This thesis has focused on the following topics:

1) To illustrate Green's functions-based calculations of electronic transmission in quantum transport. I presented a calculation of the retarded Greens' function in which simple formula of one-dimensional tight binding chain is presented and by breaking the periodicity of the lattice at a single connection it was shown that the Greens' function is related to the transmission coefficient of the scattering region.

2) Investigation of the connectivity dependence of Wigner delay time in graphene-like molecules has been studied. At first sight, it seems unreasonable that the core Green's function and corresponding magic number table can yield information about delay times, because in the absence of a magnetic field, the core Hamiltonian and corresponding Green's function $g = (E - H)^{-1}$ are real, whereas delay times are associated with the phase of the complex transmission amplitude. Nevertheless, we have demonstrated that delay time ratios can be obtained from the core Green's function or equivalently from the associated magic number tables.

3) In chapter 4 my results demonstrate that, fused porphyrin tapes substantially increase in conductance with length at moderate bias voltages, by more than a factor 10. This phenomenon is caused by the large decrease in the HOMO-LUMO gap in this system, which compensates for the increased length. In contrast, for the series of moderately-coupled butadiyne-linked wires, the conductance decays exponentially over a wide range of bias voltages, with the degree of attenuation reducing as the voltage increase. Both series, however, strongly indicate coherent transport as the dominant mechanism. This counterintuitive conductance increases with length, observed in fused porphyrins, should be a generic effect and it is likely to occur in other strongly coupled systems.

4) In chapter 5 I have studied the single-molecule conductance of a family of eight fluorene and fluorenone molecules with *para*/*meta* connectivity and thiol/pyridyl anchor groups. My results reveal that the conductance of these molecules is similar for *para* connectivity, whereas for *meta* connectivity the conductance of fluorene << fluorenone, showing the more significant role of the bridge atom for *meta* connectivity. In addition, the effect of anchor groups on single molecule conductance has been explored by using thiol and pyridine groups where, as anticipated, the conductance of the thiol anchor is much higher than the pyridine, due to the stronger interaction between thiols and gold-electrodes. The significant outcome of this work is to demonstrate that when the bridge is a methylene carbon, and the anchor groups are positioned *meta* to each other, destructive quantum interference (DQI) dominates the transport, and conductance is strongly suppressed. In complete contrast, when the bridge is a carbonyl group, the anticipated DQI is almost completely absent, and the conductance of the *meta* is only about a factor three less than the *para*, highly

surprising from a chemical standpoint. For the *meta* connectivity, this carbonyl group is cross-conjugated with each thiol and pyridyl S/N anchors atoms, such that there is no bond-alternation path connecting the two anchors (unlike in the *para* case).

6.2 Future Work

For the future, the following aspects deserve further attention:

(1) In this thesis, I have concentrated on the connectivity-dependence of Wigner delay times for electrons. For the future it would of interest to examine the connectivity-dependence of delay times for phonons[1,2] and quasi-particles associated with superconducting leads[3] , spin-dependent delay times in the presence of ferromagnetic leads or more complex metals[4,5] , combinations of superconducting and ferromagnetic leads[6,7] and the connectivity dependence of current-induced forces[8]. In practice, for such complex structures, it may not be possible to obtain simple analytic results. Nevertheless, such problems could be investigated numerically, using quantum transport codes such as the multiple-scattering code Gollum[9].

(2) Study the thermoelectric performance[10,11] in fused porphyrins also for fluorene and fluorenone core.

(3) Study the effect of using different anchor groups such as Thiol (S), Amino (NH2), Direct carbon (C), methyle sulphide (SMe), Cyano (CN) on the transport properties[12,13] for Porphyrin and fluorene and fluorenone core.

Bibliography

(1) Kambili, A.; Fagas, G.; Falko, V. I.; Lambert, C. J. Phonon-Mediated Thermal Conductance of Mesoscopic Wires with Rough Edges. *Phys. Rev. b* **1999**, *60* (23), 15593.

(2) Fagas, G.; Kozorezov, A. G.; Lambert, C. J.; Wigmore, J. K.; Peacock, A.; Poelaert, A.; Den Hartog, R. Lattice Dynamics of a Disordered Solid-Solid Interface. *Phys. Rev. b* **1999**, *60* (9), 6459.

(3) Hui, V. C.; Lambert, C. J. Andreev Scattering, Universal Conductance Fluctuations and Phase Periodic Transport. *EPL (Europhysics Lett.* **1993**, *23* (3), 203.

(4) Garc\'\ia-Suárez, V. M.; Newman, C. M.; Lambert, C. J.; Pruneda, J. M.; Ferrer, J. Optimized Basis Sets for the Collinear and Non-Collinear Phases of Iron. *J. Phys. Condens. Matter* **2004**, *16* (30), 5453.

(5) Garc\'\ia-Suárez, V. M.; Rocha, A. R.; Bailey, S. W.; Lambert, C. J.; Sanvito, S.; Ferrer, J. Single-Channel Conductance of H 2 Molecules Attached to Platinum or Palladium Electrodes. *Phys. Rev. B* **2005**, *72* (4), 45437.

(6) FalKo, V. I.; Lambert, C. J.; Volkov, A. F. Andreev Reflections and Magnetoresistance in Ferromagnet-Superconductor Mesoscopic Structures. *J. Exp. Theor. Phys. Lett.* **1999**, *69* (7), 532–538.

(7) Taddei, F.; Sanvito, S.; Jefferson, J. H.; Lambert, ad C. J. Suppression of Giant Magnetoresistance by a Superconducting Contact. *Phys. Rev. Lett.* **1999**, *82* (24), 4938.

(8) Bailey, S. W. D.; Amanatidis, I.; Lambert, C. J. Carbon Nanotube Electron Windmills: A Novel Design for Nanomotors. *Phys. Rev. Lett.* **2008**, *100* (25), 256802.

(9) Ferrer, J.; Lambert, C. J.; García-Suárez, V. M.; Manrique, D. Z.; Visontai, D.; Oroszlany, L.; Rodríguez-Ferradás, R.; Grace, I.; Bailey, S. W. D.; Gillemot, K.; et al. GOLLUM: A next-Generation Simulation Tool for Electron, Thermal and Spin Transport. *New J. Phys.* **2014**, *16*, 093029. https://doi.org/10.1088/1367-2630/16/9/093029.

(10) Reddy, P.; Jang, S.-Y.; Segalman, R. A.; Majumdar, A. Thermoelectricity in Molecular Junctions. *Science (80-.).* **2007**, *315* (5818), 1568–1571.

(11) Liu, X.; Sangtarash, S.; Reber, D.; Zhang, D.; Sadeghi, H.; Shi, J.; Xiao, Z.-Y.; Hong, W.; Lambert, C. J.; Liu, S.-X. Gating of Quantum Interference in Molecular Junctions by Heteroatom Substitution. *Angew. Chemie Int. Ed.* **2017**, *56* (1), 173–176.

(12) Frisenda, R.; Tarkuç, S.; Galán, E.; Perrin, M. L.; Eelkema, R.; Grozema, F. C.; van der Zant, H. S. J. Electrical Properties and Mechanical Stability of Anchoring Groups for Single-Molecule Electronics. *Beilstein J. Nanotechnol.* **2015**, *6*, 1558.

(13) Moreno-Garc\'\ia, P.; Gulcur, M.; Manrique, D. Z.; Pope, T.; Hong, W.; Kaliginedi, V.; Huang, C.; Batsanov, A. S.; Bryce, M. R.; Lambert, C.; et al. Single-Molecule Conductance of Functionalized Oligoynes: Length Dependence and Junction Evolution. *J. Am. Chem. Soc.* **2013**, *135* (33), 12228–12240.